ARTICLE

doi:10.1038/nature10809

Inflammasome-mediated dysbiosis regulates progression of NAFLD and obesity

Jorge Henao-Mejia[1]*, Eran Elinav[1]*, Chengcheng Jin[1,2]*, Liming Hao[3], Wajahat Z. Mehal[4], Till Strowig[1], Christoph A. Thaiss[1], Andrew L. Kau[5,6], Stephanie C. Eisenbarth[7], Michael J. Jurczak[4], Joao-Paulo Camporez[4], Gerald I. Shulman[4,8], Jeffrey I. Gordon[5], Hal M. Hoffman[9] & Richard A. Flavell[1,8]

Non-alcoholic fatty liver disease (NAFLD) is the hepatic manifestation of metabolic syndrome and the leading cause of chronic liver disease in the Western world. Twenty per cent of NAFLD individuals develop chronic hepatic inflammation (non-alcoholic steatohepatitis, NASH) associated with cirrhosis, portal hypertension and hepatocellular carcinoma, yet the causes of progression from NAFLD to NASH remain obscure. Here, we show that the NLRP6 and NLRP3 inflammasomes and the effector protein IL-18 negatively regulate NAFLD/NASH progression, as well as multiple aspects of metabolic syndrome via modulation of the gut microbiota. Different mouse models reveal that inflammasome-deficiency-associated changes in the configuration of the gut microbiota are associated with exacerbated hepatic steatosis and inflammation through influx of TLR4 and TLR9 agonists into the portal circulation, leading to enhanced hepatic tumour-necrosis factor (TNF)-α expression that drives NASH progression. Furthermore, co-housing of inflammasome-deficient mice with wild-type mice results in exacerbation of hepatic steatosis and obesity. Thus, altered interactions between the gut microbiota and the host, produced by defective NLRP3 and NLRP6 inflammasome sensing, may govern the rate of progression of multiple metabolic syndrome-associated abnormalities, highlighting the central role of the microbiota in the pathogenesis of heretofore seemingly unrelated systemic auto-inflammatory and metabolic disorders.

The prevalence of non-alcoholic fatty liver disease (NAFLD) ranges from 20–30% in the general population and up to 75–100% in obese individuals[1,2]. NAFLD is considered one of the manifestations of metabolic syndrome[3]. Whereas most patients with NAFLD remain asymptomatic, 20% progress to develop chronic hepatic inflammation (non-alcoholic steatohepatitis, NASH), which in turn can lead to cirrhosis, portal hypertension, hepatocellular carcinoma and increased mortality[4–6]. Despite its high prevalence, factors leading to progression from NAFLD to NASH remain poorly understood and no treatment has proven effective[7,8].

A "two hit" mechanism is proposed to drive NAFLD/NASH pathogenesis[9]. The first hit, hepatic steatosis, is closely associated with lipotoxicity-induced mitochondrial abnormalities that sensitize the liver to additional pro-inflammatory insults. These second hits include enhanced lipid peroxidation and increased generation of reactive oxygen species (ROS)[10]. Inflammasomes are cytoplasmic multi-protein complexes composed of one of several NLR and PYHIN proteins, including NLRP1, NLRP3, NLRC4 and AIM2. Inflammasomes are sensors of endogenous or exogenous pathogen-associated molecular patterns (PAMPs) or damage-associated molecular patterns (DAMPs)[11] that govern cleavage of effector pro-inflammatory cytokines such as pro-IL-1β and pro-IL-18 (refs 12, 13). Most DAMPs trigger the generation of ROS, which are known to activate the NLRP3 inflammasome[14]. Therefore, we propose that inflammasome-dependent processing of IL-1β and IL-18 may have an important role in the progression of NAFLD.

Results

Feeding adult mice a methionine-choline-deficient diet (MCDD) for 4 weeks beginning at 8 weeks of age induces several features of human NASH, including hepatic steatosis, inflammatory cell infiltration and ultimately fibrosis[15]. To investigate the role of inflammasomes in NASH progression, we fed MCDD to C57Bl/6 wild type (NCI), apoptosis-associated speck-like protein containing a CARD ($Asc^{-/-}$, also known as *Pycard*) and caspase 1 ($Casp1^{-/-}$) mutant mice to induce early liver damage in the absence of fibrosis (Fig. 1a–d and Supplementary Fig. 1c). Compared to wild-type animals, age- and gender-matched $Asc^{-/-}$ and $Casp1^{-/-}$ mice that were fed MCDD were characterized by significantly higher serum alanine aminotransferase (ALT) and aspartate aminotransferase (AST) activity, by enhanced microvesicular and macrovesicular hepatic steatosis, and by accumulation of multiple immune subsets in the liver from the innate and adaptive arms of the immune system (as defined by pathological examination and flow cytometry; $n = 7$–11 mice per group; Fig. 1a–d and Supplementary Figs 1c, 2a). Remarkably, the hepatic accumulation of T and B cells seems to be dispensable for this phenotype because $Asc^{-/-}$ mice lacking adaptive immune cells ($Asc^{-/-}$; $Rag^{-/-}$) also showed more severe NASH compared to wild-type animals, and comparable degrees of pathology to $Asc^{-/-}$ animals (Supplementary Fig. 2b–d).

To test whether the increased NASH observed in *Asc*- and *Casp1*-deficient mice was mediated by IL-1β or IL-18, we performed similar experiments using mice deficient in either the IL-1 receptor ($Il1r^{-/-}$)

[1]Department of Immunobiology, Yale University School of Medicine, New Haven, Connecticut 06520, USA. [2]Department of Cell Biology, Yale University School of Medicine, New Haven, Connecticut 06520, USA. [3]Department of Pathology, Yale University School of Medicine, New Haven, Connecticut 06520, USA. [4]Department of Internal Medicine, Yale University School of Medicine, New Haven, Connecticut 06520, USA. [5]Center for Genome Sciences and Systems Biology, Washington University School of Medicine, St Louis, Missouri 63108, USA. [6]Division of Allergy and Immunology, Department of Internal Medicine, Washington University School of Medicine, St Louis, Missouri 63108, USA. [7]Department of Laboratory Medicine, Yale University School of Medicine, New Haven, Connecticut 06520, USA. [8]Howard Hughes Medical Institute, Chevy Chase, Maryland 20815, USA. [9]Department of Pediatrics, Rady Children's Hospital San Diego, University of California at San Diego, La Jolla, California 92093, USA.
*These authors contributed equally to this work.

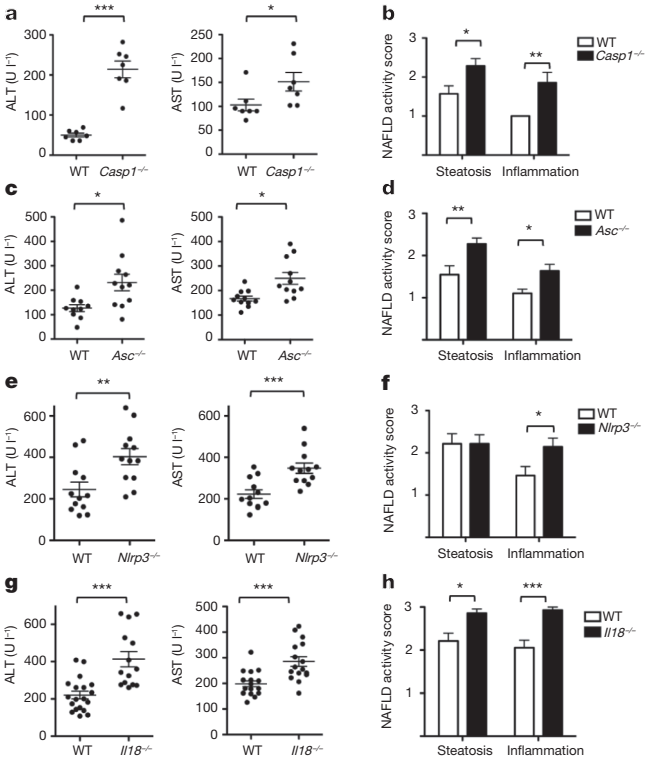

Figure 1 | Increased severity of NASH in inflammasome-deficient mice. To induce NASH, mice were fed with MCDD for 24 days. Their serum ALT and AST activities were measured and NAFLD histological activity scores were determined. **a**–**h**, Comparison of ALT, AST and NAFLD activity, plus histological scores for steatosis and inflammation between singly housed wild-type (WT) mice and *Casp1*$^{-/-}$ (**a**, **b**), *Asc*$^{-/-}$ (**c**, **d**), *Nlrp3*$^{-/-}$ (**e**, **f**), or *Il18*$^{-/-}$ (**g**, **h**). Data represent two independent experiments ($n = 7$–19 mice per treatment group). Error bars represent the s.e.m. of samples within a group. $^{*}P \leq 0.05$, $^{**}P \leq 0.01$, $^{***}P \leq 0.001$ (Student's *t*-test).

or IL-18 (*Il18*$^{-/-}$). *Il1r*$^{-/-}$ mice did not show any changes in the severity of NASH when compared to wild-type mice when fed MCDD (Supplementary Fig. 1a, b). In contrast to, but similar to *Asc*$^{-/-}$ and *Casp1*$^{-/-}$ mice, MCDD-fed *Il18*$^{-/-}$ animals featured a significant exacerbation of NASH severity (Fig. 1g, h and Supplementary Fig. 1c).

To assess the role of the NLRP3 inflammasome in NASH progression, we fed singly housed *Nlrp3*$^{-/-}$ and wild-type animals MCDD for 24 days and evaluated disease progression. *Nlrp3*$^{-/-}$ mice developed exacerbated NASH compared to wild-type mice as judged by increased levels of serum ALT and AST, plus NAFLD activity inflammation scores (Fig. 1e, f and Supplementary Fig. 1c). Remarkably, bone marrow chimaeric mice in which NLRP3 and ASC deficiency was limited to the haematopoietic compartment did not show any increase in the severity of NASH when compared to wild-type mice reconstituted with wild-type bone marrow (Supplementary Fig. 3a–f). Likewise, knock-in mice that specifically express a constitutively active NLRP3 inflammasome in CD11c^{+} myeloid cells (*Nlrp3KI*; CD11c^{+}-Cre) or hepatocytes (*Nlrp3KI*; albumin-Cre)[16] did not feature any significant differences in MCDD-induced NASH severity as compared to wild-type mice (Supplementary Fig. 3g–l). These results indicate that aberrations in inflammasome function in cells other than hepatocytes or myeloid cells are key determinants of the enhanced disease progression in inflammasome-deficient mice.

We recently discovered that inflammasomes act as steady-state sensors and regulators of the colonic microbiota, and that a deficiency in components of two inflammasomes, NLRP6 (ref. 17) and NLRP3 (unpublished), both of which include ASC and caspase 1, and involve IL-18 but not IL-1R, results in the development of an altered transmissible, colitogenic intestinal microbial community[17]. This microbiota is associated with increased representation of members of Bacteroidetes (Prevotellaceae) and the bacterial phylum TM7, and reductions in representation of members of the genus *Lactobacillus* in the Firmicutes phylum[17]. Moreover, electron microscopy studies disclosed aberrant colonization of crypts of Lieberkühn with bacteria with morphologic features of Prevotellaceae[17]. Therefore, we sought to investigate whether enhanced NASH severity in inflammasome-deficient mice is driven by their altered microbiota. Strikingly, co-housing of *Asc*$^{-/-}$ and *Il18*$^{-/-}$ mice with wild-type animals for 4 weeks (beginning at 4–6 weeks of age), before induction of NASH with MCDD resulted in significant exacerbation of NASH in the wild-type cage-mates (which we will refer to as WT(*Asc*$^{-/-}$) and WT(*Il18*$^{-/-}$), respectively, in the following text), as compared to singly housed, age- and gender-matched wild-type controls ($n = 5$–7 mice per genotype per housing condition). In co-housed wild-type mice, disease severity reached comparable levels to that of co-housed *Asc*$^{-/-}$ and *Il18*$^{-/-}$ mice (Fig. 2a–h). Moreover, significantly increased numbers of multiple inflammatory cell types were present in the liver of WT(*Asc*$^{-/-}$) compared to wild-type mice (Supplementary Fig. 2a). Similar findings were observed in wild-type mice co-housed with *Casp1*$^{-/-}$, *Nlrp3*$^{-/-}$ and *Nlrp6*$^{-/-}$ mice (Supplementary Fig. 4a–f). To exclude the possibility that aberrant microbiota presented in all mice maintained in our vivarium, we co-housed wild-type mice with other strains of NLR-deficient mice that were either obtained from the same source as *Asc*$^{-/-}$ and *Nlrp3*$^{-/-}$ mice (*Nlrc4*$^{-/-}$, *Nlrp12*$^{-/-}$), or generated in our laboratory (*Nlrp4c*$^{-/-}$). None of these strains featured a similar phenotype (Supplementary Fig. 4g–l). These results indicate that the transmissible colitogenic microbiota present in inflammasome-deficient mice is a major contributor to their enhanced NASH. In agreement with this, combined antibiotic treatment with ciprofloxacin and metronidazole, previously shown to abrogate the colitogenic activity

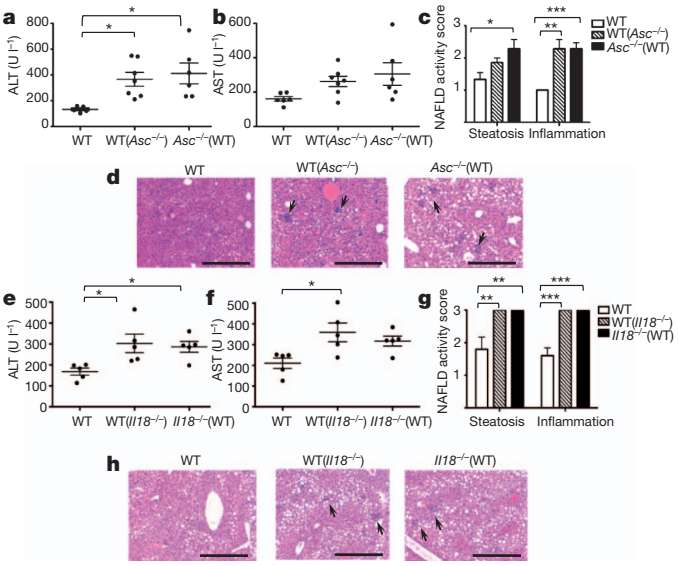

Figure 2 | Increased severity of NASH in *Asc*- and *Il18*-deficient mice is transmissible to co-housed wild-type animals. *Asc*$^{-/-}$ or *Il18*$^{-/-}$ mice and wild-type mice were co-housed for 4 weeks and then fed MCDD. **a**–**d**, ALT (**a**), AST (**b**), NAFLD activity scores (**c**), and haematoxylin and eosin-stained sections of livers (**d**) of singly housed wild-type mice (WT), wild-type mice co-housed with *Asc*$^{-/-}$ mice (WT(*Asc*$^{-/-}$)), and *Asc*$^{-/-}$ mice co-housed with wild-type mice (*Asc*$^{-/-}$(WT)). **e**–**h**, ALT (**e**), AST (**f**), NAFLD activity histological scores (**g**), and haematoxylin and eosin-stained sections of livers (**h**) of wild-type, WT(*Il18*$^{-/-}$) and *Il18*$^{-/-}$(WT). Data are representative of two independent experiments. Error bars represent s.e.m. Scale bars, 200 μm (**d**, **h**). $^{*}P \leq 0.05$, $^{**}P \leq 0.01$, $^{***}P \leq 0.001$.

of the microbiota associated with inflammasome-deficient mice associated microbiota[17], significantly reduced the severity of NASH in $Asc^{-/-}$ mice, and abolished transmission of the phenotype to WT($Asc^{-/-}$) animals (Supplementary Fig. 5).

To ascertain the effects of MCDD on the gut microbiota, we performed a culture-independent analysis of amplicons generated by primers directed against variable region 2 of bacterial 16S ribosomal RNA genes of faecal samples collected from wild-type mice co-housed with $Asc^{-/-}$ animals (WT($Asc^{-/-}$)), their $Asc^{-/-}$ cage-mates ($Asc^{-/-}$(WT)) as well as singly housed wild-type controls 1 day and 12 days before, and 7, 14 and 19 days after initiation of this diet ($n = 20$ animals; 8 singly housed wild-type, 6 co-housed wild-type and 6 $Asc^{-/-}$ mice). The structures of bacterial communities were compared based on their phylogenetic content using unweighted UniFrac. The results are illustrated in Fig. 3. Supplementary Table 1 provides a list of all phylotypes that, based on criteria outlined in Methods, discriminate co-housed WT($Asc^{-/-}$) from their singly housed wild-type counterparts. Prior to MCDD, and consistent with our previous findings[17], the faecal microbiota of WT($Asc^{-/-}$) mice adopted a configuration similar to $Asc^{-/-}$ cage-mates, including the appearance of Prevotellaceae (Supplementary Table 1 and Fig. 3 a–c). There was also a significant increase in proportional representation of members of the family Porphyromonadaceae (primarily in the genus *Parabacteroides*) in WT($Asc^{-/-}$) mice compared to their singly housed wild-type counterparts (Fig. 3d,e). The representation of Porphyromonadaceae was greatly increased in both the co-housed wild-type and $Asc^{-/-}$ mice (but not in singly housed wild-type) when they were switched to a MCDD diet ($P < 0.01$; *t*-test; Fig. 3d). A dramatic increase in the family Erysipelotrichaceae (phylum Firmicutes) also occurred with MCDD in both singly and co-housed WT animals, to a level that was >10% of the community (Fig. 3f). Although the Prevotellaceae decreased when co-housed WT($Asc^{-/-}$) mice were placed on MCDD, their relative abundance remained significantly higher than in singly housed wild-type animals (Fig. 3c).

Together, these results pointed to the possibility that members of the altered intestinal microbiota in inflammasome-deficient MCDD-treated mice may promote a signalling cascade in the liver upon translocation, resulting in progression to NASH in susceptible animals. Toll-like receptors (TLR) have a major role in NAFLD pathophysiology due to the liver's exposure to relatively large amounts of PAMPs derived from the intestine and delivered via the portal circulation[18–20]. Therefore, we propose that TLR signalling mediates the increased susceptibility to progression to NASH in mice exposed to the gut microbiota of $Asc^{-/-}$ animals. $Myd88^{-/-}$;$Trif^{-/-}$ mice are devoid of all TLR signalling pathways. When co-housed with $Asc^{-/-}$ ($Myd88^{-/-}$;$Trif^{-/-}$($Asc^{-/-}$))mice between 5 and 9 weeks of age, they showed decreased severity of NASH after exposure to MCDD for 24 days, compared to WT($Asc^{-/-}$) mice (Supplementary Fig. 6a, b).

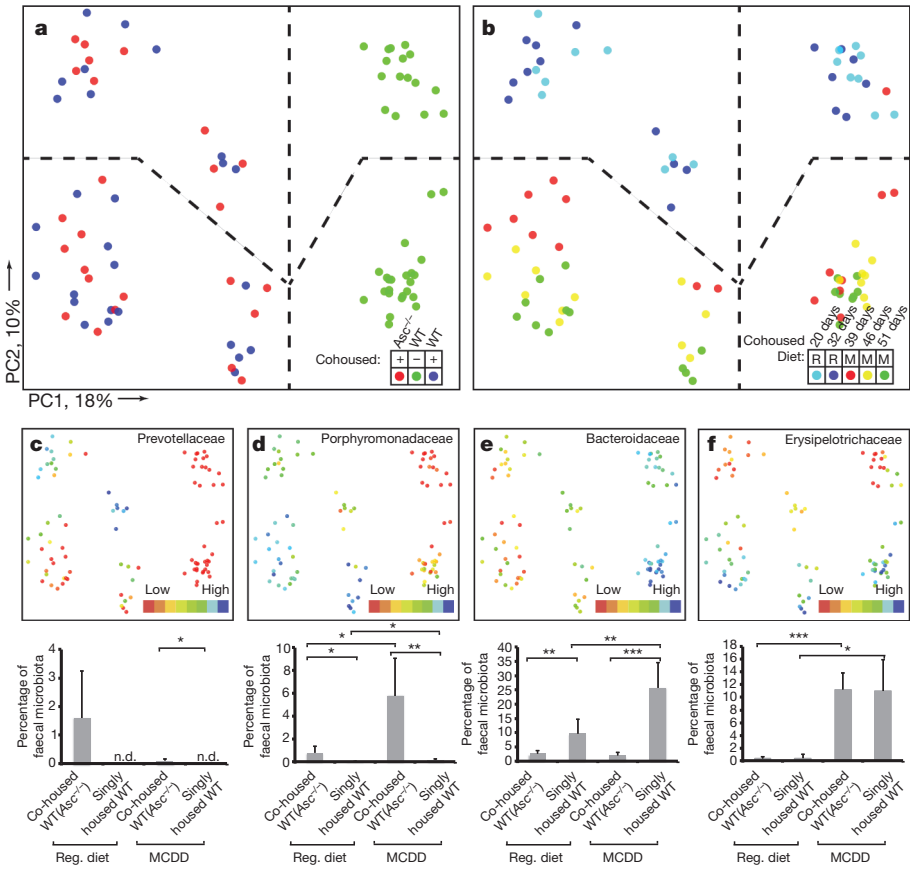

Figure 3 | 16S rRNA sequencing demonstrates diet and co-housing associated changes in gut microbial ecology. **a**, Principal coordinates analysis (PCoA) of unweighted UniFrac distances of 16S rRNA sequences demonstrating clustering according to co-housing status on principal coordinate 1 (PC1). **b**, PCoA of same plot as in **a** coloured for experimental day. Mice were co-housed and fed a regular diet (R) for the first 32 days of the experiment (two time points taken at day 20 and 32) before being switched to MCDD (M, sampled at days 39, 46 and 51 of the experiment). **c–f**, PCoA and bar graphs of family level taxa Prevotellaceae, Porphyromonadaceae, Bacteroidaceae and Erysipelotrichaceae demonstrating diet- and microbiota-dependent differences in taxonomic representation. PCoA plots contain spheres representing a single faecal community coloured according to relative representation of the taxon (blue represents relatively higher levels; red indicates lower levels). Bar graphs represent averaged taxonomic representation for singly or co-housed mouse while on either regular or MCD diet ($n = 8$ for singly housed wild-type, $n = 12$ co-housed $Asc^{-/-}$(WT) and WT($Asc^{-/-}$) animals). *$P < 0.05$, **$P < 0.01$, ***$P < 0.001$ by *t*-test after Bonferroni correction for multiple hypotheses. n.d., not detected; Reg. diet, regular diet.

To define which specific TLRs were responsible for the inflammatory response, we co-housed *Tlr4*-, *Tlr9*- or *Tlr5*-deficient mice with $Asc^{-/-}$ animals and induced NASH with MCDD as previously described. Similar to wild-type mice, $Tlr5^{-/-}$ mice co-housed with $Asc^{-/-}$ mice ($Tlr5^{-/-}(Asc^{-/-})$) featured a statistically significant exacerbation of hepatic injury, steatosis and inflammation, when compared to singly housed $Tlr5^{-/-}$ controls (Fig. 4c and Supplementary Fig. 6g, h), indicating that TLR5 does not mediate the microbiota-mediated exacerbation in disease severity. In contrast, $Tlr4^{-/-}(Asc^{-/-})$ and $Tlr9^{-/-}(Asc^{-/-})$ mice did not show the customary increase in disease severity when compared to their singly housed $Tlr4^{-/-}$ and $Tlr9^{-/-}$ counterparts (Fig. 4a, b and Supplementary Fig. 6c–f).

These observations indicate that intact bacteria or bacterial products derived from the intestine trigger TLR4 and TLR9 activation, which results in an increased rate of disease progression in mice that house a colitogenic gut microbiota associated with inflammasome deficiency (that is, $Asc^{-/-}$ and WT($Asc^{-/-}$) mice). Efforts to sequence 16S rRNA genes that might be present in total liver DNA, microbial quantitative PCR assays of portal vein blood DNA, histologic analysis of intact liver, and aerobic and anaerobic cultures of liver homogenates did not reveal any evidence of intact bacteria in wild-type or $Asc^{-/-}$ mice fed MCDD (data not shown). Notably, transmission electron microscopy studies of colon collected from wild-type and $Asc^{-/-}$ mice revealed an abundance of electron-dense material, suggestive of some black-pigmented bacterial species, in colonic epithelial cells and macrophages located in the lamina propria of $Asc^{-/-}$ mice but not in wild-type animals (Fig. 4e and Supplementary Fig. 7c). In agreement with previous results, we did not detect any translocation of intact bacteria (Fig. 4e and Supplementary Fig. 7c).

These observations provide evidence for the uptake of bacterial products from locally invasive gut microbes in $Asc^{-/-}$ mice (Fig. 4e and Supplementary Fig. 7c). If microbial components, rather than whole organisms, were transmitted to the liver then they should be detectable in the portal circulation. Indeed, levels of TLR4 and TLR9 agonists, but not TLR2 agonists (assayed by their ability to activate TLR reporter cell lines), were markedly increased in the portal circulation of MCDD-fed WT($Asc^{-/-}$), and $Asc^{-/-}$ mice compared to wild-type controls ($n = 13$–28 mice per group; Fig. 4d and Supplementary Fig. 7a, b). Altogether, these results indicate a mechanism whereby TLR4 and TLR9 agonist efflux from the intestines of inflammasome-deficient mice or their co-housed partners, through the portal circulation, to the liver where they trigger TLR4 and TLR9 activation that in turn results in enhanced progression of NASH.

We next explored the downstream mechanism whereby microbiota-induced TLR signalling enhances NASH progression. Pro-inflammatory cytokines, and in particular TNF-α, a downstream cytokine of TLR signalling, are known to contribute to progression of hepatic steatosis to steatohepatitis and eventually hepatic fibrosis in a number of animal models and in human patients[21,22]. Following induction of NASH by MCDD, hepatic *Tnf* mRNA expression was significantly upregulated in $Asc^{-/-}$ and $Il18^{-/-}$ mice, which show exacerbated disease, but not in $Il1r^{-/-}$ mice, which do not (Supplementary Fig. 8a–c). Moreover, *Tnf* mRNA levels were significantly increased in wild-type mice that had been previously co-housed with $Asc^{-/-}$ or $Il18^{-/-}$ mice and then fed MCDD (Supplementary Fig. 8d, e), indicating that its enhanced expression was mediated by elements of the microbiota responsible for NASH exacerbation. In contrast, we did not observe any changes in *Il6* or *Il1b* mRNA levels in the livers of $Asc^{-/-}$, $Il18^{-/-}$ or $Il1r^{-/-}$ mice compared to wild-type controls (Supplementary Fig. 8a–c). Furthermore, whereas MCDD-administered singly housed $Tnf^{-/-}$ mice had comparable NASH severity to singly housed wild-type animals (Fig. 4f–h and Supplementary Fig. 8f), co-housing with *Asc*-deficient mice before MCDD induction of NASH resulted in increased liver injury, hepatic steatosis and inflammation in wild-type mice but not in $Tnf^{-/-}$ mice (Fig. 4f–h and Supplementary Fig. 8f). These results indicate that TNF-α mediates the hepatotoxic effects downstream of the transmissible gut microbiota present in $Asc^{-/-}$ mice.

The aberrant gut microbiota in NLRP3 and NLRP6 inflammasome-deficient mice induces colonic inflammation through epithelial induction of CCL5 secretion[17]. To test whether this colon inflammation influences TLR agonist influx into the portal circulation and NASH progression, we induced NASH in wild-type and $Ccl5^{-/-}$ mice that had been either singly housed or co-housed. MCDD-fed, singly housed wild-type and $Ccl5^{-/-}$ mice showed equivalent levels of NASH severity (Supplementary Fig. 9a–c), indicating that CCL5 does not have a role in the early stages of NAFLD/NASH in the absence of the inflammasome-associated colitogenic microbiota. However, we documented significantly increased levels of liver injury, inflammation and steatosis in WT($Asc^{-/-}$) but not $Ccl5^{-/-}(Asc^{-/-})$ mice (Fig. 5a–c), which led us to conclude that CCL5 is required for the exacerbation of disease through cohousing with inflammasome-deficient mice. Moreover, $Ccl5^{-/-}(Asc^{-/-})$ animals showed significantly reduced levels of TLR4 and TLR9 agonists in their portal vein blood than WT($Asc^{-/-}$) mice (Supplementary Fig. 9d–f). Together, these results

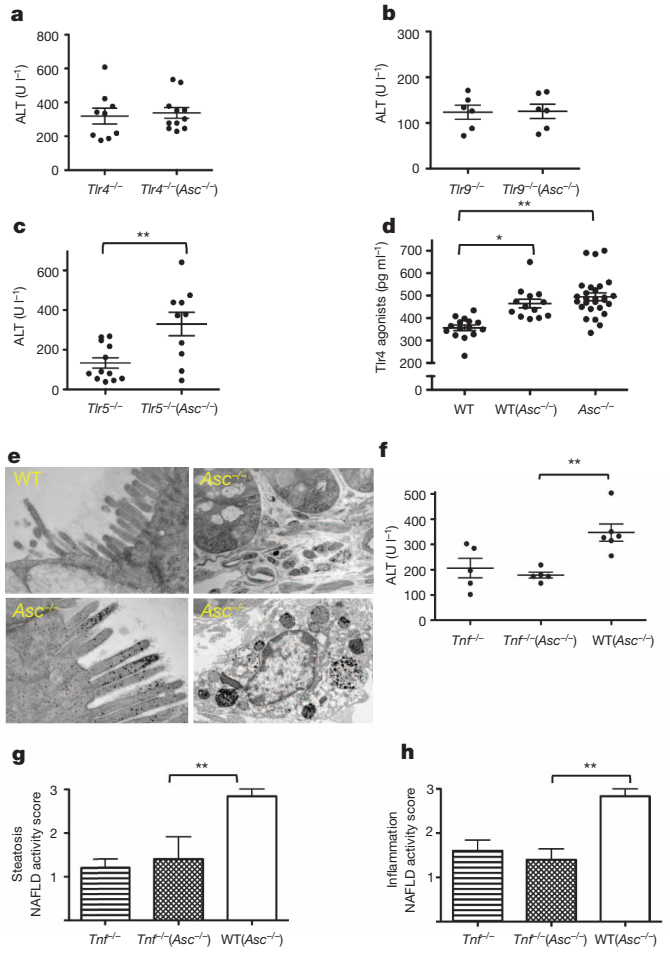

Figure 4 | Increased severity of NASH in *Asc*-deficient and co-housed wild-type animals is mediated by TLR4, TLR9 and TNF-α. $Asc^{-/-}$ mice were co-housed with wild-type, $Tnf^{-/-}$, $Tlr4^{-/-}$, $Tlr9^{-/-}$ or $Tlr5^{-/-}$ mice for 4 weeks and then fed MCDD. **a**–**c**, ALT levels of $Tlr4^{-/-}(Asc^{-/-})$ (**a**), $Tlr9^{-/-}(Asc^{-/-})$ (**b**), and $Tlr5^{-/-}(Asc^{-/-})$ mice (**c**) and their singly housed counterparts. **d**, TLR4 agonists in portal vein sera from MCDD-fed wild-type, WT($Asc^{-/-}$) and $Asc^{-/-}$ animals. **e**, Transmission electron microscopy images of colon from wild-type and $Asc^{-/-}$. **f**–**h**, ALT (**f**) and NAFLD (**g**–**h**) activity histological scores of $Tnf^{-/-}$, WT($Asc^{-/-}$) and $Tnf^{-/-}(Asc^{-/-})$ mice. Data are representative of two independent experiments. Error bars represent s.e.m. $^{*}P \leq 0.05$, $^{**}P \leq 0.01$, $^{***}P \leq 0.001$.

indicate that microbiota-induced subclinical colon inflammation is a determining factor in the rate of TLR agonist influx from the gut, and in NAFLD/NASH progression.

The MCDD system is a common model for studying inflammatory processes associated with progression from NAFLD to NASH, yet it lacks many of the associated metabolic phenotypes of NAFLD, such as obesity and insulin resistance[23]. As such, our results in this model might conceivably be limited to the way dysbiosis can influence NASH progression in patients with enhanced intestinal permeability, such as those with inflammatory bowel disease[24], but not for the majority of patients who suffer from NASH in the context of metabolic syndrome. To test whether alterations in the gut microbiota of inflammasome-deficient mice may affect the rate of progression of NAFLD and other features associated with metabolic syndrome, we extended our studies to genetically obese mice and mice fed with high-fat diet (HFD).

Leptin-receptor deficient (*db/db*; *db* is also known as *Lepr*) animals develop multiple metabolic abnormalities, including NAFLD and impaired intestinal barrier function[25], that closely resemble the human disease[26]. However, significant hepatocyte injury, inflammation, and fibrosis are not observed in the absence of a "second hit"[27]. Upon co-housing of *db/db* mice with $Asc^{-/-}$ (*db/db*($Asc^{-/-}$)) or WT mice (*db/db*(WT)) for a period of 12 weeks, and as previously shown for $Asc^{-/-}$ mice[17], the colon and ileum of all *db/db*($Asc^{-/-}$) mice showed mild to moderate mucosal and crypt hyperplasia (Fig. 5d–f) that was not seen in *db/db*(WT) mice.

Strikingly, co-housed *db/db*($Asc^{-/-}$) mice also showed increased levels of hepatocyte injury as evidenced by higher levels of ALT and AST in their sera, and significantly exacerbated steatosis and hepatic inflammation scores when compared with *db/db*(WT) mice (Fig. 5g–i). In addition to a parenchymal inflammatory exudate, patchy areas of markedly degenerated hepatocytes and hepatocytes undergoing necrosis were observed, but only in *db/db*($Asc^{-/-}$) animals (Fig. 5f). Furthermore, some areas of congestion were seen in the centro-lobular zone as well as in the hepatic parenchyma — features that resemble peliosis hepatis, a condition observed in a variety of pathological settings including infection (data not shown). In accord with our MCDD results, hepatic *Tnf* mRNA levels were significantly higher in co-housed *db/db*($Asc^{-/-}$) mice than in *db/db*(WT) animals (Fig. 5j). Again, no significant differences were observed in hepatic *Il6* or *Il1b* mRNA levels (Fig. 5j).

Interestingly, *db/db*($Asc^{-/-}$) mice developed significantly more weight gain compared to *db/db*(WT) mice after 12 weeks of co-housing (Fig. 6a), indicating that the inflammasome-associated gut microbiota could exacerbate additional processes associated with the metabolic syndrome, such as obesity. To address this possibility, we monitored multiple metabolic parameters in wild-type, WT($Asc^{-/-}$) and $Asc^{-/-}$ mice fed a high-fat diet (HFD) for 12 weeks. Strikingly, $Asc^{-/-}$ mice gained body mass more rapidly and featured enhanced hepatic steatosis (Fig. 6b, c and Supplementary Fig. 11f). $Asc^{-/-}$ mice also showed elevated fasting plasma glucose and insulin levels, and decreased glucose tolerance compared to singly housed weight-matched wild-type mice (Fig. 6d–f). Interestingly, WT($Asc^{-/-}$) mice recapitulated

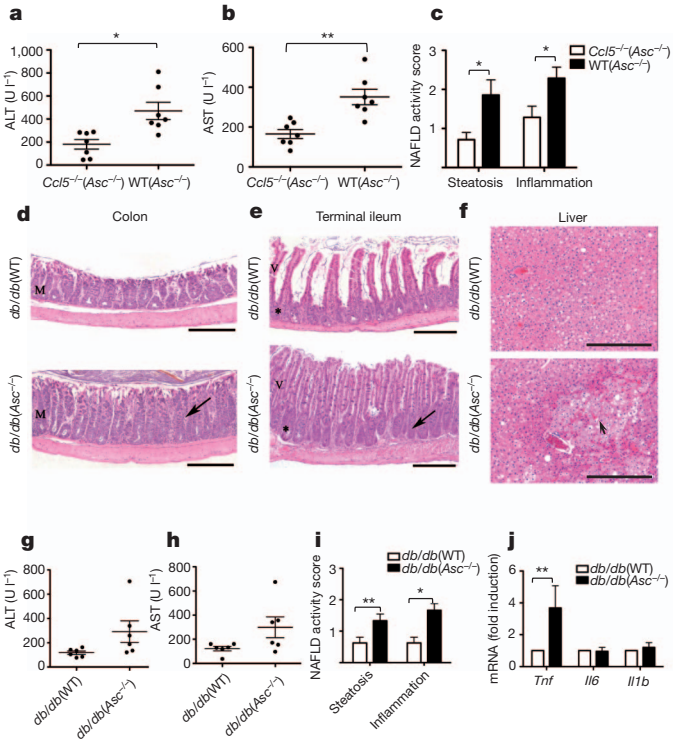

Figure 5 | Increased severity of NASH in *Asc*-deficient mice is transmissible to *db/db* by co-housing and is mediated by CCL5-induced intestinal inflammation. **a**–**c**, ALT (**a**), AST (**b**) and NAFLD (**c**) activity histological scores of WT($Asc^{-/-}$) and $Ccl5^{-/-}$($Asc^{-/-}$) mice. Data represents two independent experiments. **d**–**j**, *db/db* mice were co-housed with wild-type or $Asc^{-/-}$ mice for 12 weeks. **d**–**f**, Representative haematoxylin and eosin-stained sections of colon (**d**), terminal ileum (**e**) and liver (**f**) from *db/db*(WT) and *db/db*($Asc^{-/-}$) mice fed a standard chow diet. Mucosal and crypt hyperplasia (arrow). Hepatocyte degeneration (arrowhead). Scale bars, 500 μm (**d**–**e**), 200 μm (**f**). **g**–**i**, ALT (**g**), AST (**h**) and NAFLD (**i**) activity scores of *db/db*(WT) and *db/db*($Asc^{-/-}$) mice. **j**, Hepatic *Tnf*, *Il6* and *Il1b* mRNA levels. Error bars represent s.e.m. $*P \leq 0.05$, $**P \leq 0.01$, $***P \leq 0.001$.

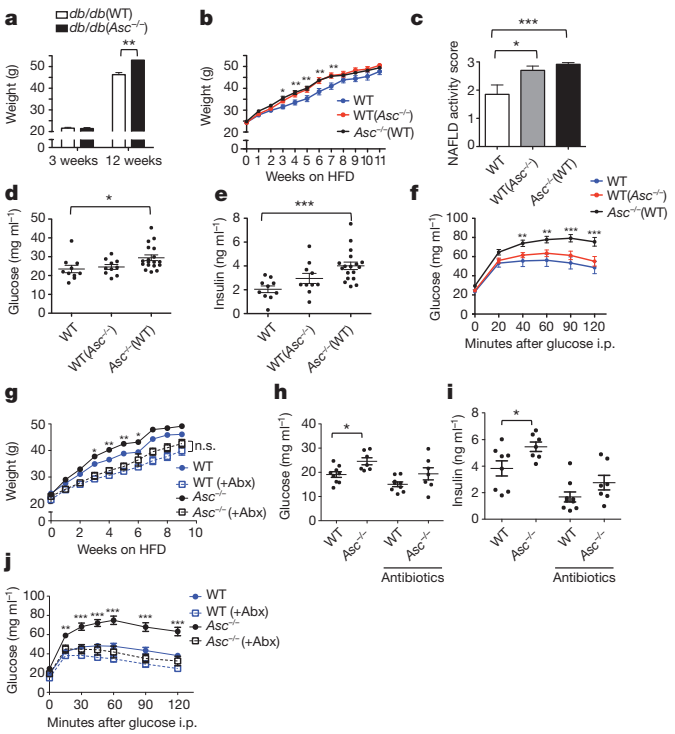

Figure 6 | *Asc*-deficient mice develop increased obesity and loss of glycaemic control on HFD. **a**, Weight of *db/db*(WT) or *db/db*($Asc^{-/-}$) mice at 3 weeks of age and at 12 weeks of co-housing. **b**–**f**, $Asc^{-/-}$ and wild-type mice were co-housed for 4 weeks and then fed HFD. **b**, Body weights. **c**, NAFLD histological activity score. **d**, **e**, Fasting plasma glucose and insulin after 11 weeks of HFD. **f**, Intraperitoneal (i.p.) glucose tolerance test after 12 weeks of HFD. **g**–**j**, Mice were untreated, or treated orally with antibiotics (Abx), for 3 weeks before HFD feeding for 12 weeks. **g**, Body weights. **h**, **i**, Fasting plasma glucose and insulin levels after 8 weeks on a HFD. **j**, Intraperitoneal glucose tolerance test after 10 weeks of HFD. Error bars represent s.e.m. $*P \leq 0.05$, $**P \leq 0.01$, $***P \leq 0.001$.

the same increased rate of body mass gain and steatosis when compared to singly housed wild-type controls, although they did not show significant alterations in glucose homeostasis (Fig. 6d–f). Nevertheless, antibiotic treatment (ciprofloxacin and metronidazole) abrogated all these abnormalities, including altered rate of gain in body mass, glucose intolerance and fasting plasma insulin levels in $Asc^{-/-}$ mice compared to wild-type mice (Fig. 6g–j). Alterations of these metabolic parameters were not caused by changes in feeding behaviour between the antibiotic-treated and untreated groups (data not shown). These results indicate different levels of microbiota-mediated regulation of the various manifestations of the metabolic syndrome: that is, some features (obesity, steatosis) are pronounced and transmissible by co-housing, whereas others (glycaemic control) are affected by alterations in the microbiota but not readily transferable by co-housing. Additionally, we performed a 16S rRNA-based analysis of the faecal microbiota of $Asc^{-/-}$ and wild-type animals that were treated with or without ciprofloxacin and metronidazole (4 weeks) before switching to HFD for 4 additional weeks. Importantly, the analysis demonstrated that Prevotellaceae and Porphyromonadaceae, two family-level taxa, were undetectable in $Asc^{-/-}$ mice 8 weeks after antibiotic treatment (Supplementary Fig. 12a–c; Supplementary Table 2).

To assess whether these metabolic abnormalities are specific to $Asc^{-/-}$ mice, we performed similar experiments with $Nlrc4^{-/-}$ mice. These mice showed an equal rate of body mass gain, and similar glucose tolerance phenotypes as singly housed wild-type mice, confirming the specificity of the phenotype (Supplementary Fig. 10a–d). 16S rRNA analysis revealed that there was an increased representation of Porphyromonadaceae in $Nlrc4^{-/-}$ mice when compared to wild-type mice (Supplementary Table 3). These results indicate that (1) some metabolic aberrations associated with the dysbiosis of inflammasome-deficient mice can be horizontally transferred from one mouse to another,(2) the gut microbiota of inflammasome-deficient mice has a negative effect on NAFLD progression and glucose homeostasis, and (3) configurational changes in the microbiota, which involve overrepresentation Porphyromonadaceae in combination with alterations in additional taxa, are likely required to produce these host phenotypes.

Discussion

The results presented here provide evidence that modulation of the intestinal microbiota through multiple inflammasome components is a critical determinant of NAFLD/NASH progression as well as multiple other aspects of metabolic syndrome such as weight gain and glucose homeostasis. Our results demonstrate a complex and cooperative effect of two sensing protein families, namely NLRs and TLRs, in shaping metabolic events. In the gut, the combination of host-related factors such as genetic inflammasome deficiency-associated dysbiosis result in abnormal accumulation of bacterial products in the portal circulation. The liver, being a 'first pass' organ and thus exposed to the highest concentration of portal system products such as PAMPs, is expected to be most vulnerable to their effects, particularly when pre-conditioned by sub-clinical pathology such as lipid accumulation in hepatocytes. Indeed in our models, accumulation of TLR agonists was sufficient to drive progression of NAFLD/NASH even in genetically intact animals.

This 'gut–liver axis', driven by alterations in gut microbial ecology, may offer an explanation for a number of long-standing, albeit poorly understood, clinical associations. One example is the occurrence of primary sclerosing cholangitis (PSC) in patients with inflammatory bowel disease, particularly those with inflammation along the length of the colon. Coeliac disease, another inflammatory disorder with increased intestinal permeability, is associated with a variety of liver disorders, ranging from asymptomatic transaminasaemia, NAFLD, to primary biliary cirrhosis (PBC). In fully developed cirrhosis, complications associated with high mortality such as portal hypertension, variceal bleeding, spontaneous bacterial peritonitis and encephalopathy are triggered by translocation of bacteria or bacterial components, providing another important example of the importance of the interplay between the microbiome, the immune response and liver pathology[28].

Recent reports suggest a complex role of inflammasome function in multiple manifestations of the metabolic syndrome. Activation of IL-1β, mainly through cleavage by the NLRP3 inflammasome, promotes insulin resistance[29,30], atherosclerotic plaque formation[31], and β cell death[32,33]. Moreover, caspase-1 activation seems to direct adipocytes towards a more insulin-resistant phenotype[34]. Conversely, *Il18*-deficient mice are prone to develop obesity, hyperphagia and insulin resistance[35]. These discrepancies most probably reflect a hierarchical contribution of multiple inflammasome components in different metabolic processes, tissues and mouse models. In agreement with previous studies, we found increased obesity and insulin resistance in *Il18*-deficient mice fed with a HFD (data not shown). However, and in contrast to two previous reports[30,34], we showed that $Asc^{-/-}$ mice are prone to obesity induction and hepatosteatosis, as well as impaired glucose homeostasis when fed a HFD. We propose that alterations in intestinal microbiota communities associated with multiple inflammasome deficiencies could account for these discrepancies and it should be added to the list of major environmental/host factors affecting manifestations and progression of metabolic syndrome in susceptible populations.

In the inflammasome-deficient setting, a significant expansion of Porphyromonadaceae was found following administration of MCDD and HFD, which was abolished by antibiotic treatment. Interestingly, one member of the family, *Porphyromonas*, has been associated with several components of the metabolic syndrome in both mice and humans, including atherosclerosis and diabetes mellitus[36,37]. Moreover, expansion of this taxa is strongly associated with complications of chronic liver disease[36]. More work is needed to further delineate the relevance of the suggested taxa discovered in our work to the pathogenesis and progression of human NAFLD/NASH and other features of the metabolic syndrome. Elucidation of similar or distinct mechanisms to the ones presented here, possibly linking Porphyromonadaceae expansion to a propensity for development of the metabolic syndrome, would be of importance to the field.

METHODS SUMMARY

Six- to eight-week-old male mice were fed a methionine-choline-deficient diet for 24 days. Eight- to ten-week-old male mice were fed a HFD ad libitum. This diet consists of 60% calories from fat and was administered for 10–12 weeks. Standard histology of liver, terminal ileum and colon were described previously[17]. The presence of immune cells in liver tissue was analysed by flow cytometry on livers digested with 0.5 mg ml^{-1} collagenase. Glucose tolerance test were performed after 10–12 weeks of consuming the HFD and mice were fasted overnight (~14 h), and injected intraperitoneally with D-glucose. Transmission electron microscopy was performed as previously described[17]. Data are expressed as mean ± s.e.m. Differences were analysed by Student's *t*-test or ANOVA and post hoc analysis for multiple group comparison. P values ≤ 0.05 were considered significant.

Full Methods and any associated references are available in the online version of the paper at www.nature.com/nature.

Received 21 April; accepted 22 December 2011.
Published online 1 February 2012.

1. Sheth, S. G., Gordon, F. D. & Chopra, S. Nonalcoholic steatohepatitis. *Ann. Intern. Med.* **126,** 137–145 (1997).
2. Ludwig, J., Viggiano, T. R., McGill, D. B. & Oh, B. J. Nonalcoholic steatohepatitis: Mayo Clinic experiences with a hitherto unnamed disease. *Mayo Clin. Proc.* **55,** 434–438 (1980).
3. Marchesini, G. *et al.* Nonalcoholic fatty liver, steatohepatitis, and the metabolic syndrome. *Hepatology* **37,** 917–923 (2003).
4. Caldwell, S. H. *et al.* Cryptogenic cirrhosis: clinical characterization and risk factors for underlying disease. *Hepatology* **29,** 664–669 (1999).
5. Shimada, M. *et al.* Hepatocellular carcinoma in patients with non-alcoholic steatohepatitis. *J. Hepatol.* **37,** 154–160 (2002).
6. Propst, A., Propst, T., Judmaier, G. & Vogel, W. Prognosis in nonalcoholic steatohepatitis. *Gastroenterology* **108,** 1607 (1995).

7. Charlton, M. Cirrhosis and liver failure in nonalcoholic fatty liver disease: molehill or mountain? *Hepatology* **47,** 1431–1433 (2008).
8. Hjelkrem, M. C., Torres, D. M. & Harrison, S. A. Nonalcoholic fatty liver disease. *Minerva Med.* **99,** 583–593 (2008).
9. Day, C. P. & James, O. F. Steatohepatitis: a tale of two "hits"? *Gastroenterology* **114,** 842–845 (1998).
10. Sanyal, A. J. *et al.* Nonalcoholic steatohepatitis: association of insulin resistance and mitochondrial abnormalities. *Gastroenterology* **120,** 1183–1192 (2001).
11. Sutterwala, F. S., Ogura, Y. & Flavell, R. A. The inflammasome in pathogen recognition and inflammation. *J. Leukoc. Biol.* **82,** 259–264 (2007).
12. Martinon, F., Burns, K. & Tschopp, J. The inflammasome. *Mol. Cell* **10,** 417–426 (2002).
13. Agostini, L. *et al.* NALP3 forms an IL-1β-processing inflammasome with increased activity in Muckle-Wells autoinflammatory disorder. *Immunity* **20,** 319–325 (2004).
14. Zhou, R., Yazdi, A. S., Menu, P. & Tschopp, J. A role for mitochondria in NLRP3 inflammasome activation. *Nature* **469,** 221–225 (2011).
15. Varela-Rey, M. *et al.* Non-alcoholic steatohepatitis and animal models: understanding the human disease. *Int. J. Biochem. Cell Biol.* **41,** 969–976 (2009).
16. Brydges, S. D. *et al.* Inflammasome-mediated disease animal models reveal roles for innate but not adaptive immunity. *Immunity* **30,** 875–887 (2009).
17. Elinav, E. *et al.* NLRP6 inflammasome regulates colonic microbial ecology and risk for colitis. *Cell* **145,** 745–757 (2011).
18. Rivera, C. A. *et al.* Toll-like receptor-4 signaling and Kupffer cells play pivotal roles in the pathogenesis of non-alcoholic steatohepatitis. *J. Hepatol.* **47,** 571–579 (2007).
19. Miura, K. *et al.* Toll-like receptor 9 promotes steatohepatitis by induction of interleukin-1β in mice. *Gastroenterology* **139,** 323–334 e7 (2010).
20. Seki, E. *et al.* TLR4 enhances TGF-β signaling and hepatic fibrosis. *Nature Med.* **13,** 1324–1332 (2007).
21. Crespo, J. *et al.* Gene expression of tumor necrosis factor α and TNF-receptors, p55 and p75, in nonalcoholic steatohepatitis patients. *Hepatology* **34,** 1158–1163 (2001).
22. Li, Z. *et al.* Probiotics and antibodies to TNF inhibit inflammatory activity and improve nonalcoholic fatty liver disease. *Hepatology* **37,** 343–350 (2003).
23. Diehl, A. M. Lessons from animal models of NASH. *Hepatol. Res.* **33,** 138–144 (2005).
24. Broomé, U., Glaumann, H. & Hultcrantz, R. Liver histology and follow up of 68 patients with ulcerative colitis and normal liver function tests. *Gut* **31,** 468–472 (1990).
25. Guo, X. *et al.* Leptin signaling in intestinal epithelium mediates resistance to enteric infection by *Entamoeba histolytica*. *Mucosal Immunol.* **4,** 294–303 (2011).
26. Ikejima, K. *et al.* The role of leptin in progression of non-alcoholic fatty liver disease. *Hepatol. Res.* **33,** 151–154 (2005).
27. Guebre-Xabier, M. *et al.* Altered hepatic lymphocyte subpopulations in obesity-related murine fatty livers: potential mechanism for sensitization to liver damage. *Hepatology* **31,** 633–640 (2000).
28. Almeida, J., Galhenage, S., Yu, J., Kurtovic, J. & Riordan, S. M. Gut flora and bacterial translocation in chronic liver disease. *World J. Gastroenterol.* **12,** 1493–1502 (2006).
29. Vandanmagsar, B. *et al.* The NLRP3 inflammasome instigates obesity-induced inflammation and insulin resistance. *Nature Med.* **17,** 179–188 (2011).
30. Wen, H. *et al.* Fatty acid-induced NLRP3-ASC inflammasome activation interferes with insulin signaling. *Nature Immunol.* **12,** 408–415 (2011).
31. Duewell, P. *et al.* NLRP3 inflammasomes are required for atherogenesis and activated by cholesterol crystals. *Nature* **464,** 1357–1361 (2010).
32. Zhou, R., Tardivel, A., Thorens, B., Choi, I. & Tschopp, J. Thioredoxin-interacting protein links oxidative stress to inflammasome activation. *Nature Immunol.* **11,** 136–140 (2010).
33. Masters, S. L. *et al.* Activation of the NLRP3 inflammasome by islet amyloid polypeptide provides a mechanism for enhanced IL-1β in type 2 diabetes. *Nature Immunol.* **11,** 897–904 (2010).
34. Stienstra, R. *et al.* Inflammasome is a central player in the induction of obesity and insulin resistance. *Proc. Natl Acad. Sci. USA* **108,** 15324–15329 (2011).
35. Netea, M. G. *et al.* Deficiency of interleukin-18 in mice leads to hyperphagia, obesity and insulin resistance. *Nature Med.* **12,** 650–656 (2006).
36. Bajaj, J. S. *et al.* Linkage of gut microbiome with cognition in hepatic encephalopathy. *Am. J. Physiol. Gastrointest. Liver Physiol.* **302,** 168–175 (2011).
37. Makiura, N. *et al.* Relationship of *Porphyromonas gingivalis* with glycemic level in patients with type 2 diabetes following periodontal treatment. *Oral Microbiol. Immunol.* **23,** 348–351 (2008).

Supplementary Information is linked to the online version of the paper at www.nature.com/nature.

Acknowledgements We thank E. Eynon, J. Alderman, A. Williams, F. Manzo and H. Elinav for technical assistance and discussions; M. Graham and C. Rahner for performing electron microscopy; D. R. Peaper for assistance in microbiological culture procedures; R. Sherwin for helpful advice; X. Fan for technical assistance; Yale Diabetes Endocrinology Research Center and Mouse Metabolic Phenotyping Center for assistance with the metabolic analysis. E.E. is supported by the Cancer Research Institute (2010-2012) and by a supplementary grant from the Israel-US educational foundation (2009) and is a recipient of the Claire and Emmanuel G. Rosenblatt award from the American Physicians for Medicine in Israel Foundation (2010-2011). J.H.M. and T.S. are supported by Leukemia and Lymphoma Society Postdoctoral Fellowships. S.C.E. is supported by T32HL007974 and K08A1085038. W.Z.M. is supported by R01DK076674-01 and the VA Merit award. This work was supported in part by the Howard Hughes Medical Institute (G.I.S., R.A.F.), the United States-Israel binational Foundation grant (E.E. and R.A.F.), the Crohn's and Colitis Foundation of America (A.K. and J.I.G.) and R01 DK-40936, R24 DK-085638, P30 DK-45735 and U24 DK-059635 The authors report no conflict of interest.

Author Contributions J.H.-M., E.E. and R.A.F. designed the study and wrote the manuscript. J.H.-M., E.E., C.J., L.H., W.Z.M., M.J.J., J.-P.C., G.I.S. and C.A.T. performed the *in vitro* and *in vivo* experimental work and edited the manuscript. T.S. and S.C.E. supported the work with key suggestions and editing of the manuscript. H.M.H. provided the *Nlrp3* knock-in mice and provided valuable feedback on the manuscript. A.L.K. and J.I.G. performed the stool processing and metagenomic analysis of the microbiota and provided key suggestions to the manuscript and participated in its editing. R.A.F. directed the project.

Author Information 16S rRNA data sets have been deposited in MG-RAST under accession number qiime:909. Reprints and permissions information is available at www.nature.com/reprints. The authors declare no competing financial interests. Readers are welcome to comment on the online version of this article at www.nature.com/nature. Correspondence and requests for materials should be addressed to R.A.F. (richard.flavell@yale.edu).

METHODS

Mice. *Casp1*$^{-/-}$ (Casp1^{tm1Flv}) and *Nlrp4c*$^{-/-}$ mice were generated in our laboratory[38]. Production of *ASC*$^{-/-}$ (Pycard^{tm1Flv}), *Nlrp3*$^{-/-}$, *Nlrp6*$^{-/-}$, *Nlrc4*$^{-/-}$ and *Nlrp12*$^{-/-}$ mice is described elsewhere[17]. *Il18*$^{-/-}$ (Il18^{tm1Aki}), *Il1r*$^{-/-}$ (Il1r1^{tm1Imx}), *Tnf*$^{-/-}$ (Tnf^{tm1Gkl}), *Tlr4*$^{-/-}$ (Tlr4$^{lps\text{-}del}$), *Tlr5*$^{-/-}$ (Tlr5^{tm1Flv}), *Myd88*$^{-/-}$ (Myd88^{tm1Defr}), *Ccl5*$^{-/-}$(Ccl5^{tm1Hso}), *Rag1*$^{-/-}$ (Rag1^{tm1Mom}), CD11c-Cre (Itgax-cre), albumin-Cre (Alb-cre), *Trif*$^{-/-}$ (*Ticam1*^{Lps2}) and *db/db*(*Lepr*^{db}) mice were obtained from Jackson Laboratories. *Tlr9*$^{-/-}$ mice have been described in another report[39]. Production of *Nlrp3KI* (A350V) mice is described elsewhere[16]. Wild-type C57Bl/6 mice were purchased from the NCI. For co-housing experiments, age-matched wild-type and KO mice at the age of 4–6 weeks were co-housed in sterilized cages for 4 or 12 weeks at a ratio of 1:1 (WT:KO), with unrestricted access to food and water. No more than 6 mice in total were housed per cage. For antibiotic treatment, mice were given a combination of ciprofloxacin (0.2 g l^{-1}) and metronidazole (1 g l^{-1}) for 4 weeks in the drinking water. All antibiotics were obtained from Sigma Aldrich. All experimental procedures were approved by the local IACUC.

NASH model. 6–8 week-old male mice were fed a methionine-choline-deficient diet (MP Biomedicals) for 24 days. Methionine-choline-sufficient control diet was the same but supplemented with choline chloride (2 g per kg of diet) and DL-methionine (3 g per kg of diet). Mice had unrestricted access to food and water.

High fat diet model. 8-10 week-old male mice were fed a HFD ad libitum. This diet consists of 60% calories from fat (D12492i; Research Diets) and was administered for 10–12 weeks.

Histology. The intact liver was excised immediately after mice were euthanized by asphyxiation, fixed in 10% neutral buffered formalin and embedded in paraffin. Liver sections were stained with haematoxylin and eosin, or trichrome. Histological examination was performed in a blinded fashion by an experienced gastrointestinal pathologist with the histological scoring system for NAFLD[40]. Briefly, steatosis and inflammation scores ranged from 0 to 3 with 0 being within normal limits and 3 being most severe. Individual scores were assigned for each parameter. The most severe area of hepatic inflammation of representative histology sections were photographed using an Olympus microscope.

Colons were fixed in Bouin's medium and embedded in paraffin. Blocks were serially sectioned along the cephalocaudal axis of the gut to the level of the lumen; 5-μm-thick sections were stained with haematoxylin and eosin. Digital light microscopic images were recorded with a Zeiss Axio Imager.A1 microscope, AxioCam MRc5 camera and AxioVision 4.7.1 imaging software (Carl Zeiss Microimaging). Further details in ref. 17.

Gene expression analysis. Tissues were preserved in RNAlater solution (Ambion), and subsequently homogenized in TRIzol reagent (Invitrogen). RNA (1 μg) was used to generate complementary DNA using the HighCapacity cDNA Reverse Transcription kit (Applied Biosystems). Real time PCR was performed using gene-specific primer/probe sets (Applied Biosystems) and Kapa Probe Fast qPCR kit (Kapa Biosystems) on a 7500 Fast Real Time PCR instrument (Applied Biosystems). The reaction conditions were 95 °C for 20 s, followed by 40 cycles of 95 °C for 3 s and 60 °C for 30 s. Data was analysed using the Sequence Detection Software according to the ΔC_t method with *Hprt* serving as the reference housekeeping gene.

Glucose tolerance test (GTT). GTTs were performed after 10–12 weeks of consuming the HFD. Mice were fasted overnight (~14 h), and injected intraperitoneally with 10% dextrose at a dose of 1 g per kg body weight. Blood was collected from tail vein and plasma glucose levels measured at indicated times using a YSI 2700 Select Glucose Analyzer (YSI Life Sciences). Plasma insulin levels were determined by radioimmunoassay (Linco).

Flow cytometry analysis. Livers were collected, digested with 0.5 mg ml^{-1} collagenase IV (Sigma) for 45 min at 37 °C, homogenized and repeatedly centrifuged at 400*g* for 5 min to enrich for haematopoietic cells. Cells were stained for flow cytometry using antibodies against CD45.2, CD11b, CD11c, NK1.1, B220, CD4, CD8, TCRβ, F4/80, Gr-1, MHC class II (Biolegend) and analysed on a BD LDR II.

Portal vein blood collection. Mice were anaesthetized with ketamine 100 mg per kg and xylazine 10 mg per kg. Mice were placed on a clean surgical field, and the abdominal fur was clipped and cleaned with a two stage surgical scrub consisting of Betadine and 70% ethanol. A 1 to 1.5 cm midline incision was made in the skin and abdominal wall. The peritoneum was moved to the left and the portal vein was punctured with a 30G needle. Between 0.2 and 0.3 ml of blood were collected per mouse. Serum was recovered by centrifugation at 1,500*g* for 15 min at room temperature and then stored at −80 °C in endotoxin-free tubes until assayed.

Measurement of PAMPs. TLR2, TLR4 and TLR9 agonists were assayed in portal vein serum using HEK-blue mTLR2, HEK-blue mTLR4 and HEK-blue mTLR9 reporter cell lines (InvivoGen) and the manufacturer's protocol with modifications. In brief, 2.2×10^5 HEK-blue mTLR2, 1.0×10^5 HEK-blue mTLR4 and 2.0×10^5 HEK-blue mTLR9 cells were plated in 96-well plates containing 10 μl of heat-inactivated (45 min at 56 °C) portal vein serum. Cells were then incubated for 21 h at 37 °C under an atmosphere of 5% CO_2/95% air. Twenty microlitres of the cell culture supernatants were collected and added to 180 μl of the QUANTI-Blue substrate in a 96-well plate. The mixtures were then incubated at 37 °C in 5% CO_2/95% air for 3 h and secreted embryonic alkaline phosphatase levels were determined using a spectrophotometer at 655 nm.

Transmission electron microscopy. Mice were perfused via their left ventricles using 4% paraformaldehyde in PBS. Selected tissues were fixed in 2.5% glutaraldehyde in 0.1 M sodium cacodylate buffer pH 7.4 for 1–2 h. Samples were rinsed three times in sodium cacodylate buffer and post-fixed in 1% osmium tetroxide for 1 h, en bloc stained in 2% uranyl acetate in maleate buffer pH 5.2 for a further hour then rinsed, dehydrated, infiltrated with Epon812 resin, and baked overnight at 60 °C. Hardened blocks were cut using a Leica UltraCut UCT. 60-nm-thick sections were collected and stained using 2% uranyl acetate and lead citrate. Samples were all viewed in an FEI Tencai Biotwin TEM at 80 kV. Images were taken using Morada CCD and iTEM (Olympus) software. Further details in ref. 17.

Bone marrow chimeras. Bone marrow was flushed from femurs with DMEM with 10% FBS, red cells were lysed, and the material filtered through a 70 μm filter. 10^6 cells in 100 μl PBS were delivered by retro-orbital injection into lethally irradiated (1,000 rad) mice. For 2 weeks post-engraftment, mice were maintained on antibiotics (Sulfatrim). Six weeks after transplantation animals were switched to MCDD. A wild-type non-irradiated mouse was co-housed with the engrafted mice for 4 weeks before NASH induction. Under our standardized protocol, bone marrow chimaeras routinely show a level of engraftment of ≥ 93%.

Bacterial 16S rRNA amplicon sequencing. Total DNA was isolated from the livers of mice fed a MCDD diet and used for attempted PCR amplification of variable region 2 of bacterial16S rRNA genes[20] that may be present in the tissue. Thirty cycles of amplification of liver DNA prepared from seven wild-type, and seven *Asc*$^{-/-}$ mice yielded detectable product (>60 ng per reaction) in three samples from the wild-type group and three samples from the *Asc*$^{-/-}$ group. All amplicons were then subjected to multiplex pyrosequencing with a 454 instrument using FLX Titanium chemistry (137–1,510 reads per sample, average read length, 360 nucleotides). Reads were analysed using the QIIME software package. Operational taxonomic unit (OTU) picking was performed using uclust and taxonomic assignments made with RDP[41]. This analysis demonstrated inconsistent representation of taxa between animals and taxa that largely represented organisms not associated with the gut microbiota. G-test indicated that there was no significant correlation between any of these taxa and the presence of NASH.

For analysis of the faecal microbiota of MCDD-fed *Asc*$^{-/-}$(WT), WT(*Asc*$^{-/-}$) and singly housed wild-type mice, faecal pellets were collected at the time points indicated in Fig. 3. The protocols that we used to extract faecal DNA and to perform multiplex pyrosequencing of amplicons generated by PCR from the V2 regions of bacterial 16S rRNA genes, have been previously described[20]. A total of 366,283 sequences were generated from 181 faecal samples (average 2,023 ± 685 reads per sample; average read length, 360 nucleotides). Sequences were de-multiplexed and binned into species-level operational taxonomic units (OTUs; 97% nucleotide sequence identity; %ID) using QIIME 1.2.1 (ref. 41). Taxonomy was assigned within QIIME using RDP. Chimaeric sequences were removed using ChimeraSlayer and OTUs were filtered to a minimum of 10 sequences per OTU and 1,000 OTUs per sample. PCoA plots were generated by averaging the unweighted UniFrac distances of 100 subsampled OTU tables. Statistical analysis was performed on the proportional representation of taxa (summarized to Phyla, Class, Order, Family and Genus levels), using paired (where possible) and unpaired *t*-tests. Taxa that were significantly different after multiple hypothesis testing were included in Supplementary Tables 1–3.

Statistical analysis. Data are expressed as mean ± s.e.m. Differences were analysed by Student's *t*-test or ANOVA and post hoc analysis for multiple group comparison. *P* values ≤ 0.05 were considered significant.

38. Sutterwala, F. S. *et al.* Critical role for NALP3/CIAS1/Cryopyrin in innate and adaptive immunity through its regulation of caspase-1. *Immunity* **24,** 317–327 (2006).
39. Hemmi, H. *et al.* A Toll-like receptor recognizes bacterial DNA. *Nature* **408,** 740–745 (2000).
40. Kleiner, D. E. *et al.* Design and validation of a histological scoring system for nonalcoholic fatty liver disease. *Hepatology* **41,** 1313–1321 (2005).
41. Caporaso, J. G. *et al.* QIIME allows analysis of high-throughput community sequencing data. *Nature Methods* **7,** 335–336 (2010).

doi:10.1038/nature10809

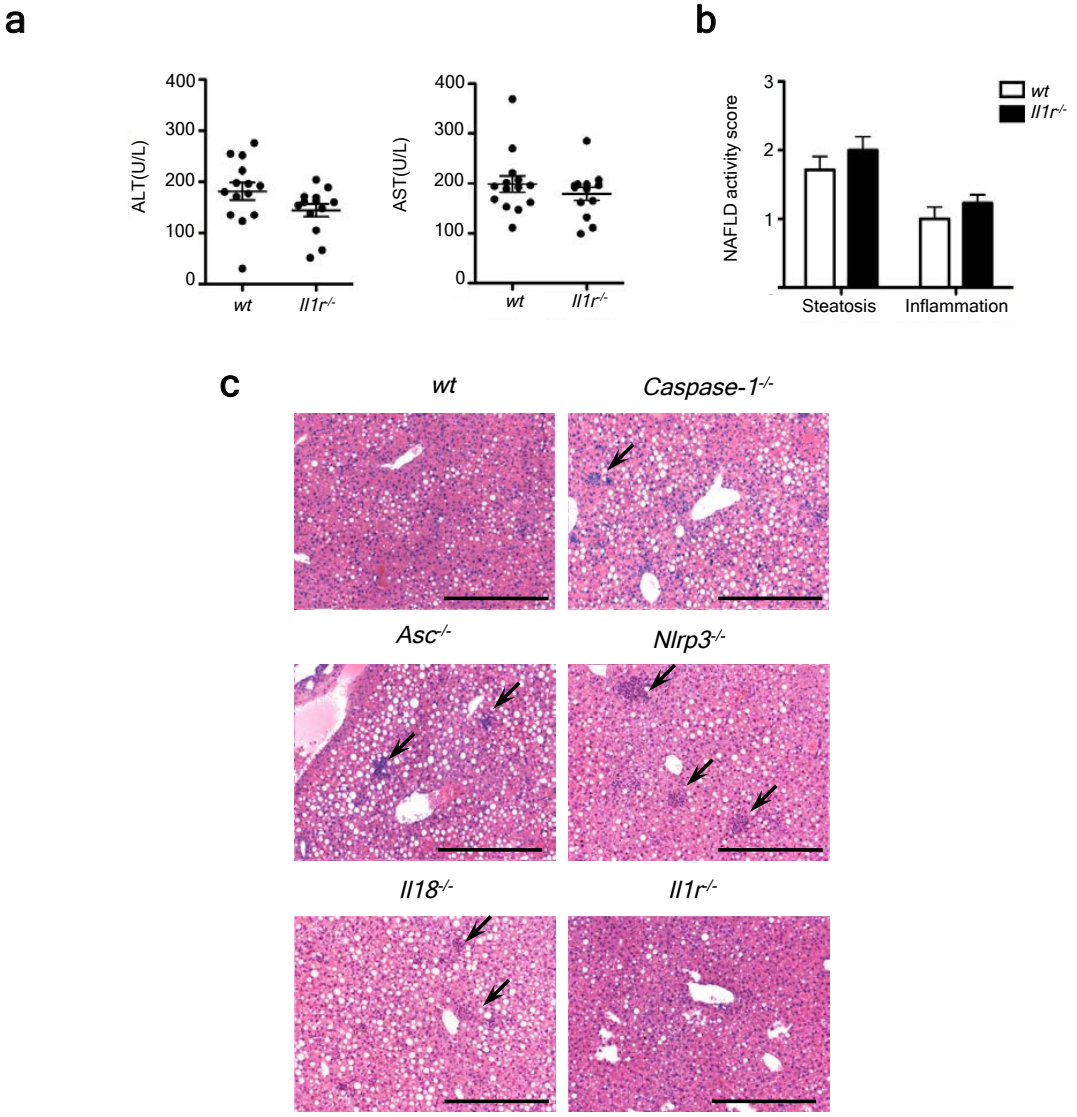

Supplemental figure 1. Increased severity of NASH in inflammasome-deficient mice, but not in *Il1r*-deficient animals. To induce NASH, mice were fed with MCDD for 24 d. Their serum ALT and AST activities measured and NAFLD histological activity scores were determined. (**a-b**) Comparison of ALT, AST, and NAFLD activity, plus histological scores for steatosis and inflammation between singly-housed wild-type (*wt*) mice and *Il1r*$^{-/-}$ animals. (**c**) Representative hematoxylin and eosin (H&E)-stained sections of livers from *wt*, *caspase-1*$^{-/-}$, *Asc*$^{-/-}$, *Nlrp3*$^{-/-}$, *Il18*$^{-/-}$, and *Il1r*$^{-/-}$ mice. Inflammatory foci are highlighted with an arrowhead. Data represent two independent experiments (n=7-19 mice/treatment group). Error bars represent the SEM of samples within a group. Scale bars = 200 μm (**K**). *p≤ 0.05, **p≤ 0.01, ***p≤ 0.001 (Student's t test).

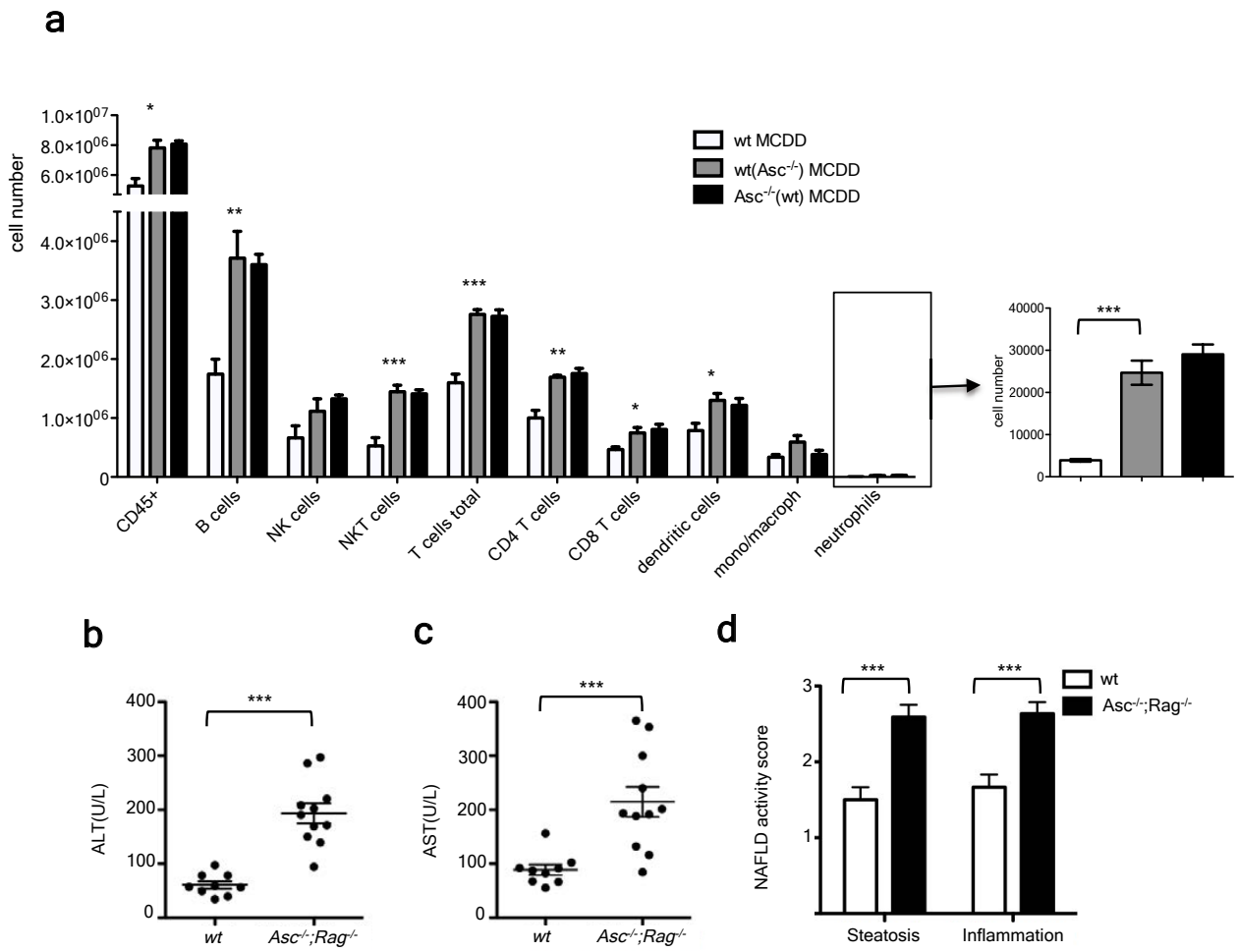

Supplemental figure 2. Changes in liver cellularity in MCDD-fed *Asc*-deficient mice and cohoused *wt* animals. Singly-housed *wt*, co-housed *Asc*$^{-/-}$ (*wt*), and co-housed *wt*(*Asc*$^{-/-}$) animals were fed MCDD for 24 d to induce NASH, and hematopoietic cell subsets in liver were quantified by FACS. (**a**) Total numbers of CD45+ cells, B cells (B220^{+}), T cells (TCRβ^{+}), CD4+ T cells, CD8+ T cells, NK cells (NK1.1^{+} TCRβ^{-}), NKT cells (NK1.1^{+} TCRβ^{+}), dendritic cells (CD11c^{+} CD11b^{-}), mononuclear macrophages (MHCII^{+} CD11b^{+}), and neutrophils (Gr1^{+}). *p≤ 0.05, **p≤ 0.01, ***p≤ 0.001 between the *wt* single housed group and the co-housed *wt*(*Asc*$^{-/-}$) animals (Student's t test). Data is prepresentative of two independent experiments. (**b-d**) Comparison of serum ALT, serum AST, plus NAFLD activity histological scores for steatosis and inflammation in *wt* and compound homozygous knockout *Asc*$^{-/-}$;*Rag*$^{-/-}$ mice. Error bars represent the SEM of samples within a group. *p≤ 0.05, **p≤ 0.01, ***p≤ 0.001 (Student's t test).

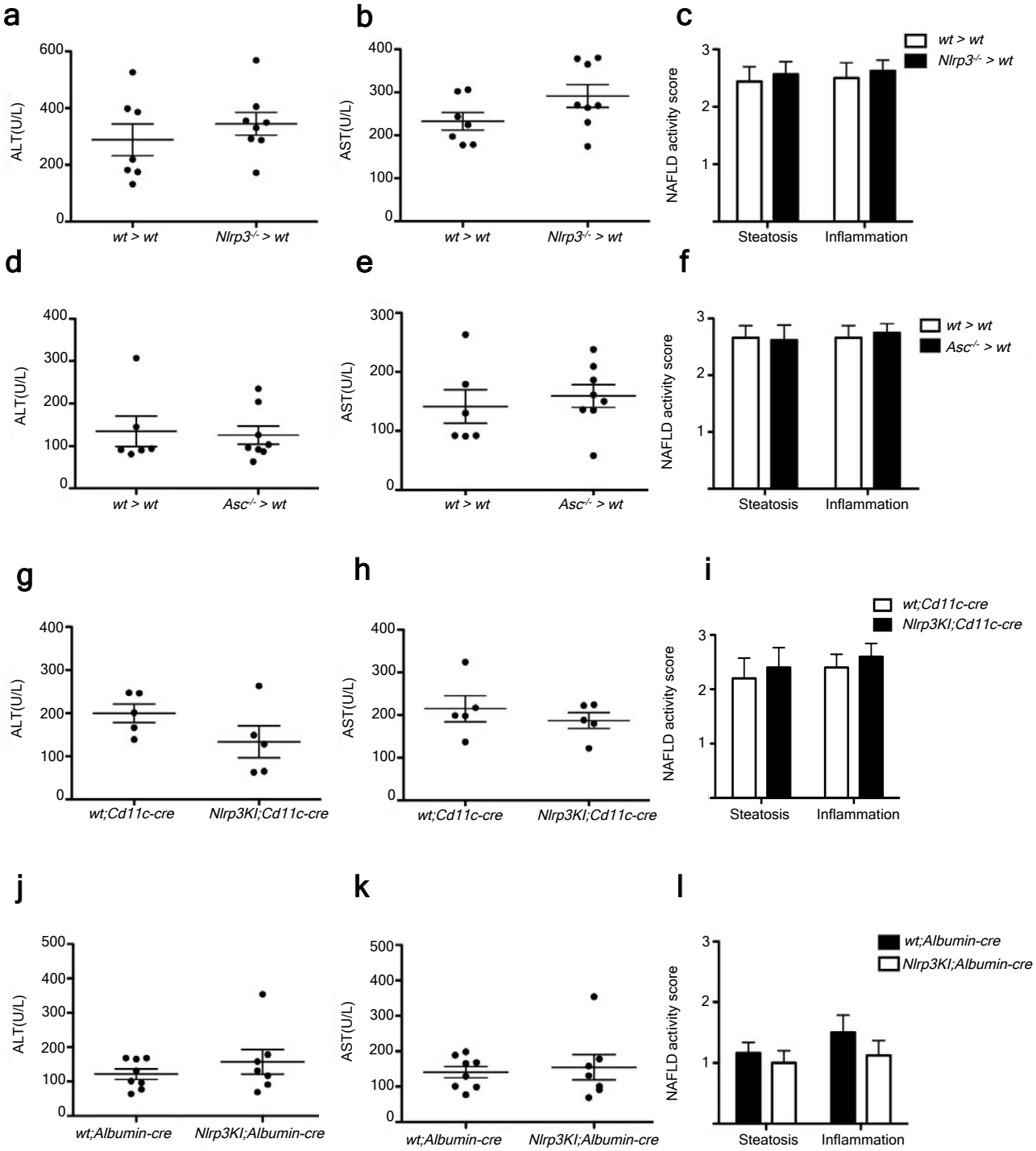

Supplemental figure 3. Activation of the NLRP3 inflammasome in hematopoietic cells and hepatocytes does not influence NASH severity. To induce NASH, mice were given MCDD for 24 d, and their serum ALT and AST activities, and NAFLD histological activity scores were determined. (**a-f**) Comparison of ALT, AST, and NAFLD activity histological scores for steatosis and inflammation between chimeric mice generated with *wt* (*wt* > *wt*) and *Nlrp3*$^{-/-}$ (*Nlrp3*$^{-/-}$>*wt*) bone marrow (BM) (**a-c**) or *Asc*$^{-/-}$ (*Asc*$^{-/-}$>*wt*) BM (**d-f**). (**g-l**) Comparison of serum ALT and AST activities, and NAFLD activity histological scores for steatosis and inflammation between *wt*;CD11c+-Cre and *Nlrp3KI*;CD11c-Cre mice (**g-i**) or *wt*;albumin-Cre and *Nlrp3KI*;albumin-Cre mice (**j-l**) . Error bars represent the SEM of samples within a group. *p≤ 0.05, **p≤ 0.01, ***p≤ 0.001. (Student's t test)

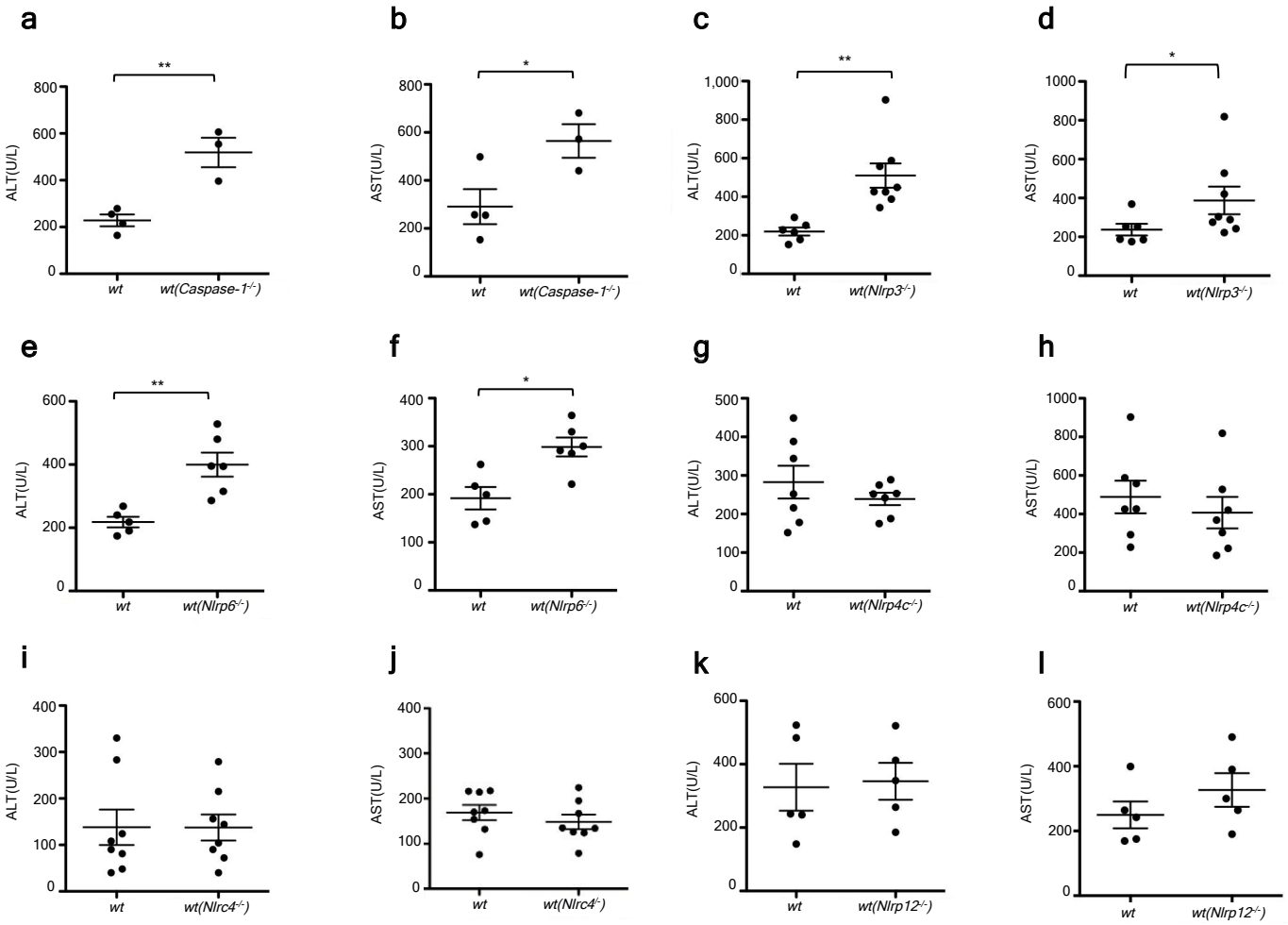

Supplemental figure 4. Increased severity of NASH in *caspase-1*-, *Nlrp3*-, and *Nlrp6*-deficient mice is transmissible to co-housed wild-type animals. Singly-housed *wt* (*wt*) mice and *wt* mice co-housed with *caspase-1*$^{-/-}$ animals (*wt* (*caspase-1*$^{-/-}$)) (**a,b**), *Nlrp3*$^{-/-}$ animals (*wt*(*Nlrp3*$^{-/-}$)) (**c,d**), *Nlrp6*$^{-/-}$ animals (*wt*(*Nlrp6*$^{-/-}$)) (**e,f**), *Nlrp4c*$^{-/-}$ mice (*wt*(*Nlrp4c*$^{-/-}$)) (**g,h**), *Nlrc4*$^{-/-}$ mice (*wt*(*Nlrc4*$^{-/-}$)) (**i,j**), and *Nlrp12*$^{-/-}$ mice (*wt*(*Nlrp12*$^{-/-}$)) (**k,l**) were given MCDD for 24 d to induce NASH. Comparison of serum ALT and AST activities in *wt* and *wt*(*caspase-1*$^{-/-}$) (**a,b**), *wt*(*Nlrp3*$^{-/-}$) (**c,d**), *wt*(*Nlrp6*$^{-/-}$) (**e,f**), *wt*(*Nlrp4c*$^{-/-}$) (**g,h**), *wt*(*Nlrc4*$^{-/-}$) (**i,j**), and (*wt*(*Nlrp12*$^{-/-}$)) animals (**k,l**). Error bars represent the SEM of samples within a group (n=3-8 mice/group). *p≤ 0.05, **p≤ 0.01, ***p≤ 0.001. (Student's t test)

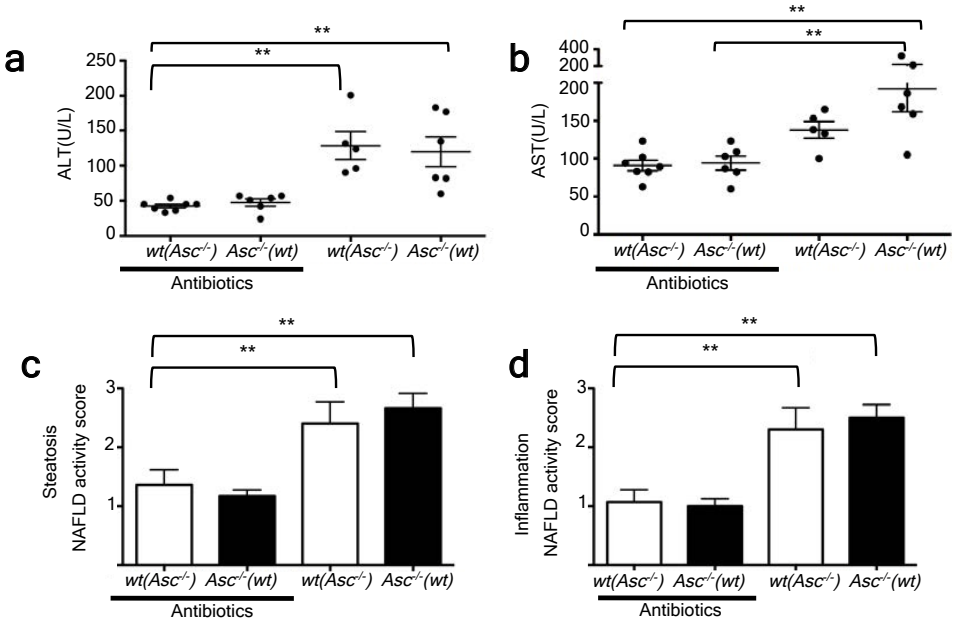

Supplemental figure 5. The increased severity of NASH in *Asc* and *Il18*-deficient mice and co-housed wild-type animals is abolished with antibiotic treatment. (**a-d**) Comparison of serum ALT (**a**) and AST (**b**), plus NAFLD activity histological scores for steatosis (**c**) and inflammation (**d**) of *wt* (*Asc*$^{-/-}$) and *Asc*$^{-/-}$(*wt*) mice that were untreated or treated orally with a combination of metronidazole and ciprofloxacin for 4 weeks. Inflammatory foci are highlighted with an arrowhead. Data are represents two independent experiments (n=5-7 mice/treatment group). Error bars represent the SEM of samples within a group. *p≤ 0.05, **p≤ 0.01, ***p≤ 0.001. (ANOVA)

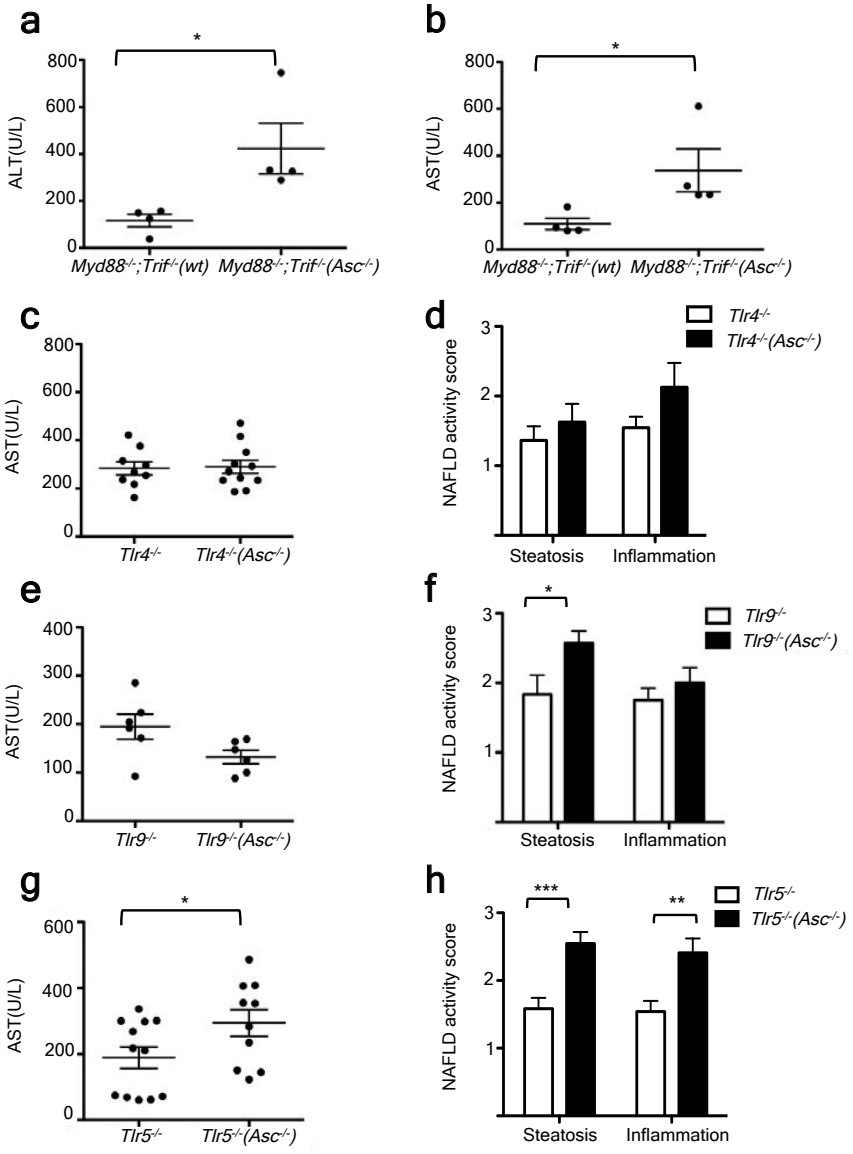

Supplemental figure 6. Increased severity of NASH in *Asc*-deficient mice and co-housed wild-type animals is mediated by TLR4, TLR9. *Asc*$^{-/-}$ mice were co-housed with *wt*, *Myd88*$^{-/-}$*;Trif*$^{-/-}$, *Tlr4*$^{-/-}$, *Tlr9*$^{-/-}$, or *Tlr5*$^{-/-}$ mice for 4 weeks, after which time mice were fed MCDD for 24 days to induce NASH. (**a-b**) Comparison of serum ALT and AST activities from MCDD-fed *wt*(*Asc*$^{-/-}$) and *Myd88*$^{-/-}$*;Trif*$^{-/-}$(*Asc*$^{-/-}$) mice. Data are representative of two independent experiments. (**c-h**) Comparison of serum AST levels and NAFLD activity histological scores for steatosis and inflammation from MCDD-fed *Tlr4*$^{-/-}$(*Asc*$^{-/-}$) (**c-d**), *Tlr9*$^{-/-}$(*Asc*$^{-/-}$) (**e-f**), and *Tlr5*$^{-/-}$(*Asc*$^{-/-}$) animals (**g-h**) and their singly-housed counterparts. Data represent two independent experiments. Error bars represent the SEM of samples within a group. *p≤ 0.05, **p≤ 0.01, ***p≤ 0.001 (Student's t test).

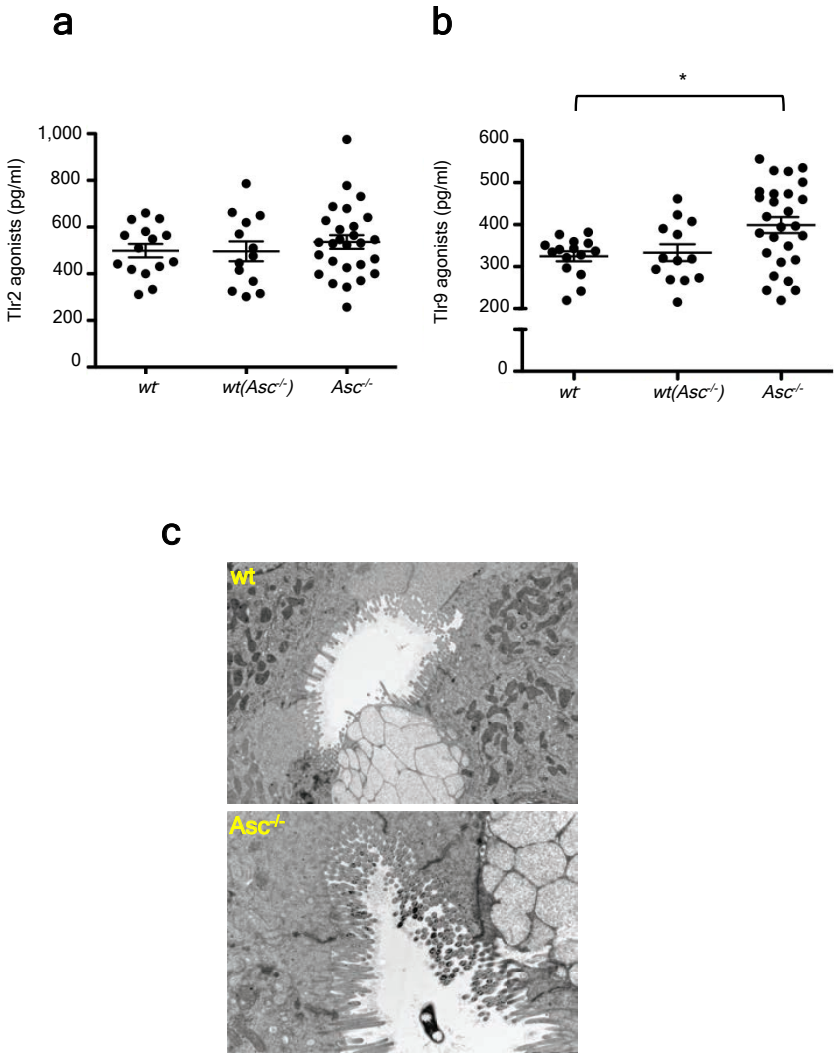

Supplemental figure 7. Increased severity of NASH in *Asc*-deficient mice and co-housed wild-type animals is mediated by TLR agonist influx into portal circulation. *Asc*$^{-/-}$ mice were co-housed with *wt* mice for 4 weeks, after which time mice were fed MCDD for 24 days to induce NASH. (**a-b**) Comparison of TLR2 (**a**) and TLR9 (**b**) agonists in portal vein sera obtained at the time of sacrifice of singly-housed MCDD-fed *wt* mice, co-housed *wt*(*Asc*$^{-/-}$) animals and singly-housed *Asc*$^{-/-}$ animals. Data represent two independent experiments. (**c**) Representative transmission electron microscopy images taken from colonic sections prepared from *wt* (top X8200) and *Asc*$^{-/-}$ animals (bottom left X16500). Error bars represent the SEM of samples within a group. *p≤ 0.05, **p≤ 0.01, ***p≤ 0.001. (ANOVA)

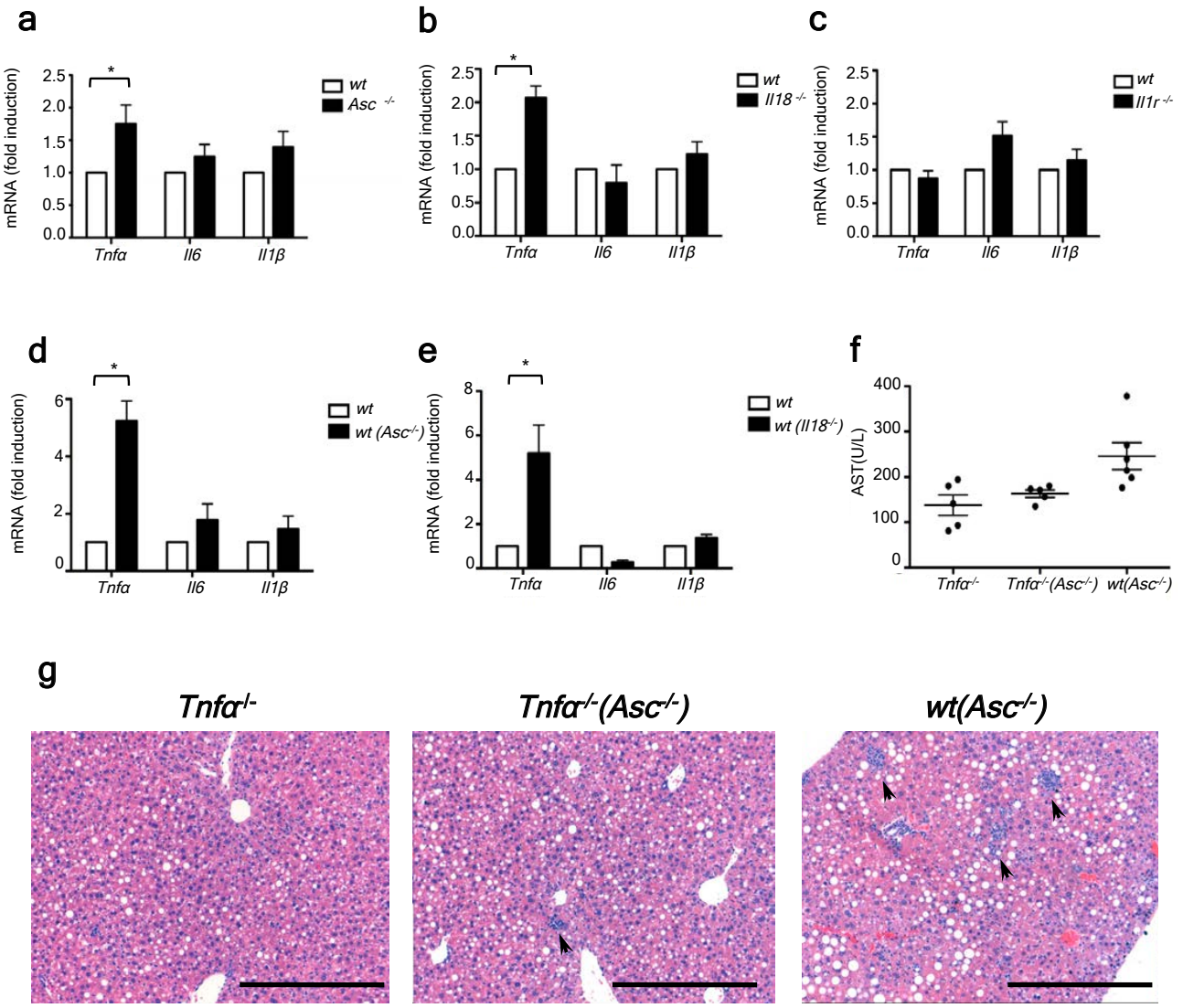

Supplemental figure 8. Increased *Tnfα* expression in *Asc*$^{-/-}$, *Il18*$^{-/-}$, but not in *Il1r*$^{-/-}$ mice during NASH. (**a-c**) Comparison of hepatic *Tnfα, Il6*, and *Il1β* mRNA levels in singly-housed *wt* and *Asc*$^{-/-}$(**a**), *Il18*$^{-/-}$(**b**), or *Il1r*$^{-/-}$(**c**) mice. (**d-e**) Comparison of hepatic *Tnfα, Il6,* and *Il1β* mRNA levels in singly-housed *wt* mice (*wt*) versus *wt* mice that were previously co-housed with *Asc*$^{-/-}$ animals (*wt*(*Asc*$^{-/-}$)) (**d**), or *Il18*$^{-/-}$ animals (*wt*(*Il18*$^{-/-}$))(**e**) for four weeks prior to NASH induction. (**f-g**) AST serum levels (**f**) and representative H&E-stained sections of livers from singly-housed *Tnfα* $^{-/-}$ mice, and co-housed *wt* mice (*wt*(*Asc*$^{-/-}$) or *Tnfα* $^{-/-}$ mice co-housed with *Asc*$^{-/-}$ animals (*Tnfα* $^{-/-}$(*Asc*$^{-/-}$). Scale bars = 200 μm. Data are representative for two independent experiments. Error bars represent the SEM of samples within a group. *p≤ 0.05, **p≤ 0.01, ***p≤ 0.001. (Student's t test)

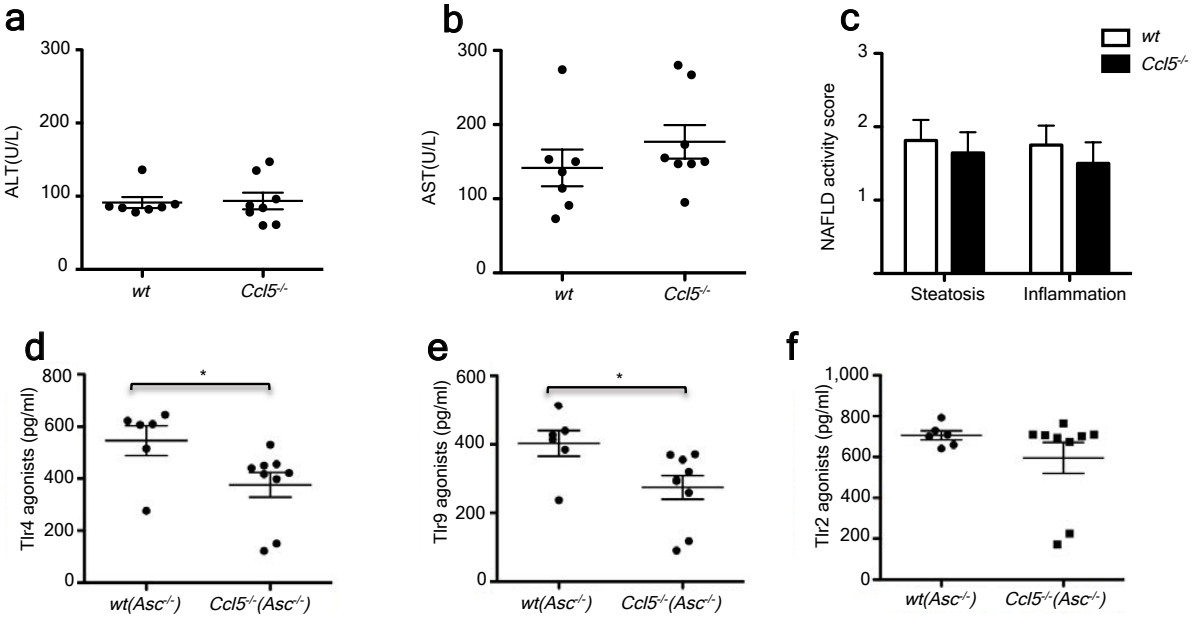

Supplementary figure 9. Intestinal inflammation associated with an *Asc*$^{-/-}$ gut microbiota increases the influx of TLR agonists into the portal circulation. To induce NASH, mice were given MCDD for 24 d, and their serum ALT and AST activities, and NAFLD histological activity scores were determined. (**a-c**) Comparison of ALT (**a**), AST (**b**), and NAFLD activity histological scores for steatosis and inflammation (**c**) between separately housed *wt* and *Ccl5*$^{-/-}$ mice. (n=8 animals surveyed/group). (**d-f**) *wt* or *Ccl5*$^{-/-}$ mice were co-housed with *Asc*$^{-/-}$ mice for 4 weeks after which time mice were fed MCDD for 24 d to induce NASH. Comparison of TLR4 (**d**), TLR9 (**e**), and TLR2 (**f**) agonists in portal vein sera collected from MCDD-treated, co-housed *wt*(*Asc*$^{-/-}$) and *Ccl5*$^{-/-}$(*Asc*$^{-/-}$) mice. Error bars represent the SEM of samples within a group (n=6 animals surveyed/group). *p≤ 0.05, **p≤ 0.01, ***p≤ 0.001 (Student's t test).

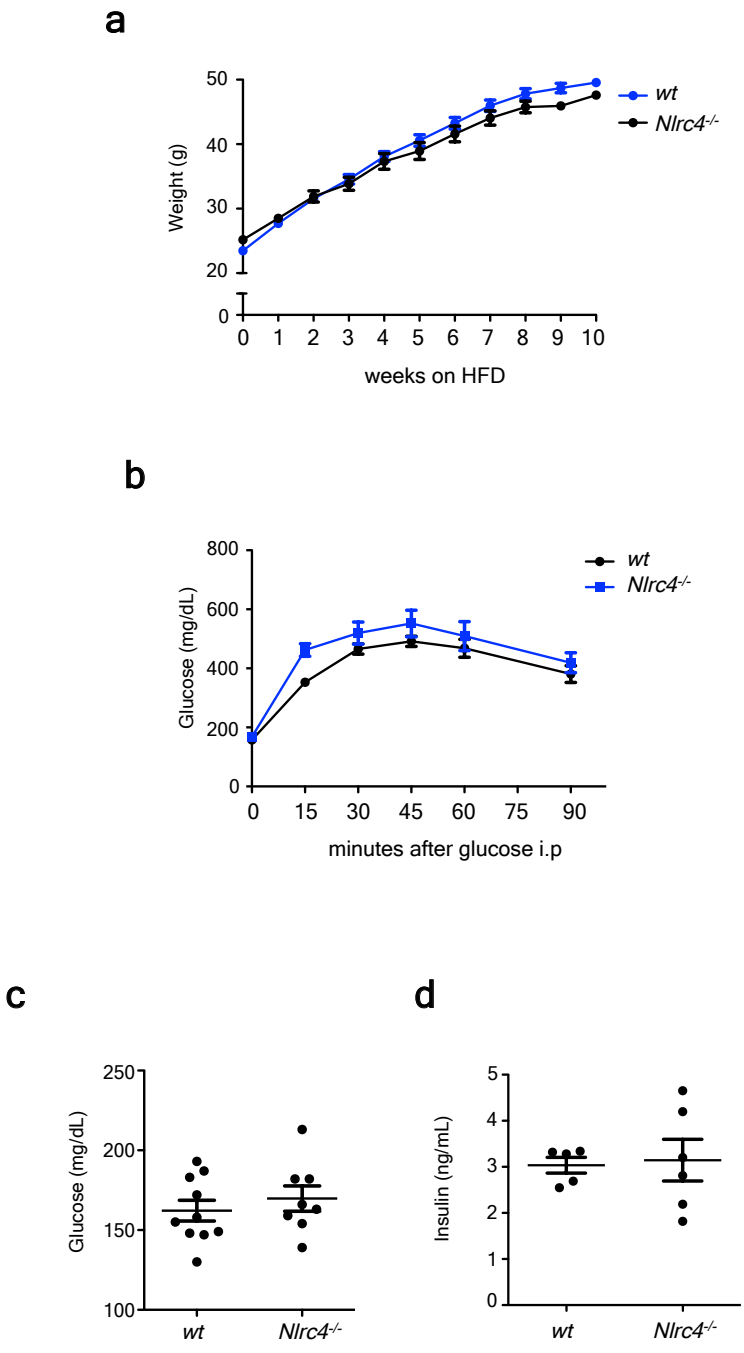

Supplementary figure 10. ***Nlrc4*-deficient mice have normal weight gain rate and glycemic control on HFD.** Age-matched male *Nlrc4*$^{-/-}$ mice and *wt* mice were fed a 60% HFD. Body weights were monitored weekly (**a**), glucose tolerance tests were performed in *wt* mice and *Nlrc4*$^{-/-}$ mice after 10 weeks of HFD (**b**). Fasting (14h) blood glucose (**c**) and insulin (**d**) levels were measured after 8 weeks on the HFD, (n=8-10 mice/group). Error bars represent the SEM of samples within a group.

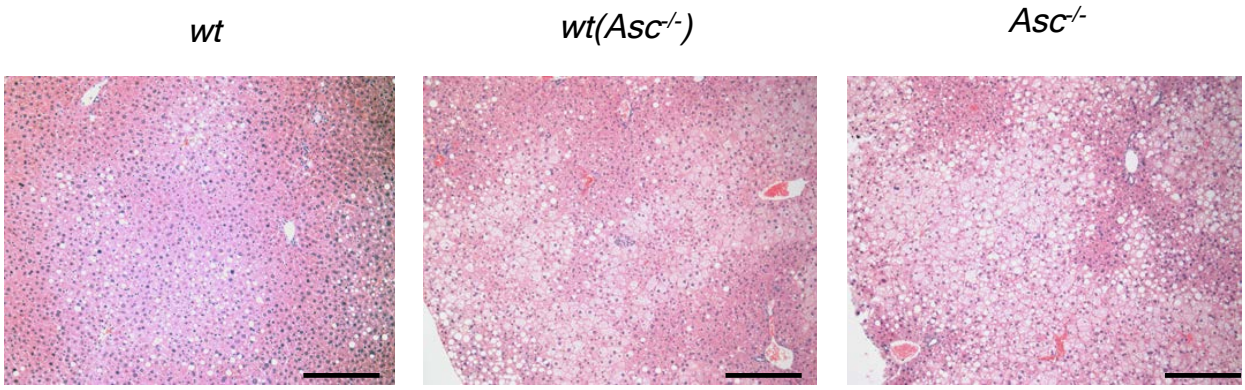

Supplemental figure 11. *Asc*-deficient mice co-housed *wt* mice develop increased steatosis on HFD. (**a**) Representative hematoxylin and eosin (H&E)-stained sections of livers from *wt*, *wt*(*Asc*$^{-/-}$), and *Asc*$^{-/-}$ mice. Scale bars = 200 μm.

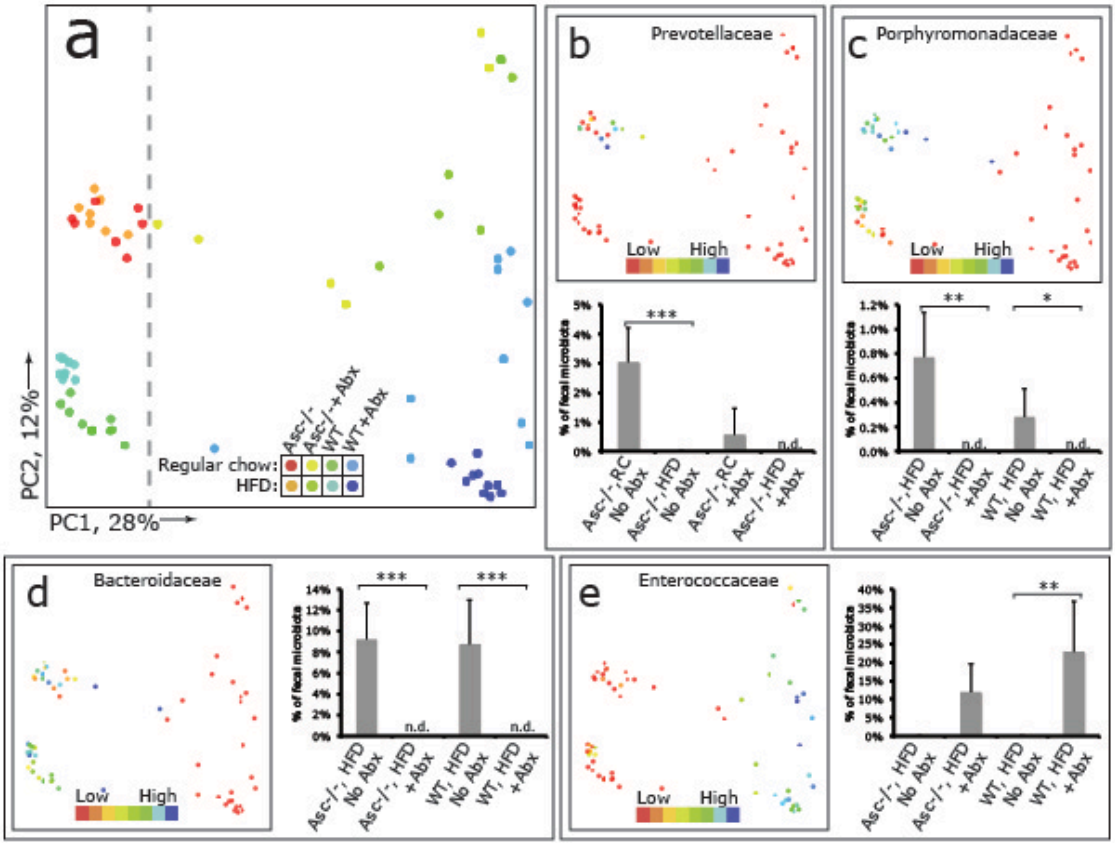

Supplemental figure 12. Antibiotic treatment leads to reduction in taxa associated with HFD. (**a**) *Asc-/-* and WT mice were or were not treated with ciprofloxacin and metronidazole for 4 weeks before being switched to a high fat diet. Time points were taken after being fed HFD for 1 and 8 weeks. (**b-e**) PCoA and bar graphs showing reduction in Prevotellaceae, Porphyromonadaceae and Bacteroidaceae after antibiotic treatment. Enterococcaceae were noted to increase in representation after antibiotic treatment.